Some forms of acquired TTP (e.g., idiopathic TTP, ticlopidine-induced TTP) are associated with the production of autoantibodies against ADAMTS13.

Recently, murine models of ADAMTS13 deficiency have been developed by gene-targeting technique by two independent groups [2, 3]. Models resulting from a naturally occurring mutation have also been established [4]. These animal models have proven useful to elucidate ADAMTS13 functions in vivo and the pathophysiology of TTP. This review summarizes phenotypic characteristics of *Adamts13*-mutant mice, focusing on roles of ADAMTS13 in thrombosis, endotoxemia and inflammation.

2 The gene structure of mouse *Adamts13*

In mice, two kinds of *Adamts13* gene are present in a strain-specific manner (Fig. 1) [5]. The *Adamts13* gene of the 129/Sv, FVB/NJ, and CAST/EiJ strains contains 29 exons like the human *ADAMTS13* gene and encodes ADAMTS13 protein with the same domain constitutions as human ADAMTS13, designated as ADAMTS13-L. On the other hand, several strains of mice, including the BALB/c, C3H/He, C57BL/6, and DBA/2 strains, harbor the insertion of an intracisternal A-particle (IAP) retrotransposon into intron 23 of the *Adamts13* gene. The inserted IAP is one of the endogenous transposable elements present at approximately 2,000 sites in the mouse genome. Like retroviruses, the IAP contains two long terminal repeats with signals for the initiation and regulation of transcription and for the polyadenylation of transcripts. The IAP insertion into the *Adamts13* gene produces a cryptic splicing site followed by a premature in-frame stop codon and a polyadenylation signal derived from the long terminal repeat. As a result, ADAMTS13 protein that lacks the C-terminal two thrombospondin type 1 motif (Tsp1) domains and two CUB domains, designated as ADAMTS13-S, is predominantly expressed in these strains.

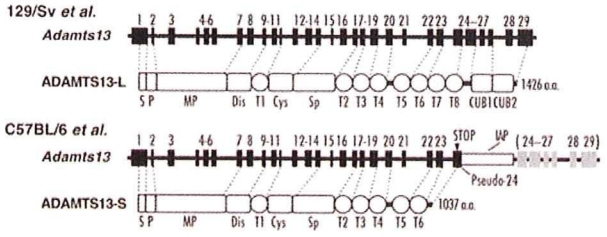

Fig. 1 Gene and protein structure of two kinds of mouse ADAMTS13. In some strains of mice (e.g., C57BL/6), an IAP-retrotransposon (*IAP*) is inserted into intron 23 of the *Adamts13* gene (*arrow*) and creates a pseudo-exon 24 including a premature stop codon. ADAMTS13-S with truncated C-terminal domains is mainly expressed in these strains. *S* Signal peptide, *P* propeptide, *MP* metalloprotease domain, *Dis* disintegrin-like domain, *T* (*numbered 1-8*) thrombospondin type 1 motif domain, *Cys* cysteine-rich domain, *Sp* spacer domain, *CUB* complement components C1r/C1 s, urchin epidermal growth factor, and bone morphogenic protein-1 domain

Both forms of mouse ADAMTS13 are mainly expressed in the liver and retain a furin-recognition sequence in the propeptide domain, a Zn^{2+}-coordinating active site sequence, the Met residue in a proposed Met-turn, and structural Ca^{2+} coordination residues in the metalloprotease domain, and an RGD sequence in the Cys-rich domain. They show VWF-cleaving activity in vitro but the truncated form exhibits lower activity than the full-length form for purified human VWF multimers [6].

3 Generation of ADAMTS13-deficient mice

Mice deficient in ADAMTS13 have been developed by conventional gene-targeting approaches. Banno et al. generated *Adamts13*$^{-/-}$ mice on a 129/Sv genetic background [2]. Disruption of the gene by replacing exons 3–6, encoding the metalloprotease domain, with a neomycin resistance cassette results in the absence of ADAMTS13 mRNA in liver. ADAMTS13 activity is not detected in plasma of *Adamts13*$^{-/-}$ mice. Analysis of plasma VWF multimer patterns detects UL-VWF multimers in *Adamts13*$^{-/-}$ mice but not in *Adamts13*$^{+/+}$ or *Adamts13*$^{+/-}$ mice, suggesting that the deficiency of ADAMTS13 alone can support the generation of plasma UL-VWF multimers. However, *Adamts13*$^{-/-}$ mice are viable with no apparent signs of TTP. Blood platelet counts, plasma haptoglobin levels and peripheral blood smears are normal in *Adamts13*$^{-/-}$ mice, suggesting a lack of thrombocytopenia and hemolytic anemia. Although pregnancy is a triggering event for TTP, *Adamts13*$^{-/-}$ females survive pregnancy and produce viable offspring of normal-sized litters. Renal histology of pregnant *Adamts13*$^{-/-}$ mice does not show thrombi deposition or excessive VWF accumulation in microvessels.

Motto et al. [3] have generated *Adamts13*$^{-/-}$ mice with elimination of exons 1–6. On a mixed C57BL/6J and 129X1/SvJ genetic background, they are viable without any TTP-like phenotypes, similar to *Adamts13*$^{-/-}$ mice on a 129/Sv genetic background. Thus, both studies clearly indicate that ADAMTS13 deficiency alone is not sufficient to cause TTP-like symptoms in mice. Factors in addition to ADAMTS13 deficiency may be necessary for the development of TTP in mice.

4 The function of ADAMTS13 in thrombosis

4.1 Increased thrombogenesis in ADAMTS13-deficient mice

While *Adamts13*$^{-/-}$ mice do not spontaneously develop TTP, they are in prothrombotic state. Banno et al. revealed that

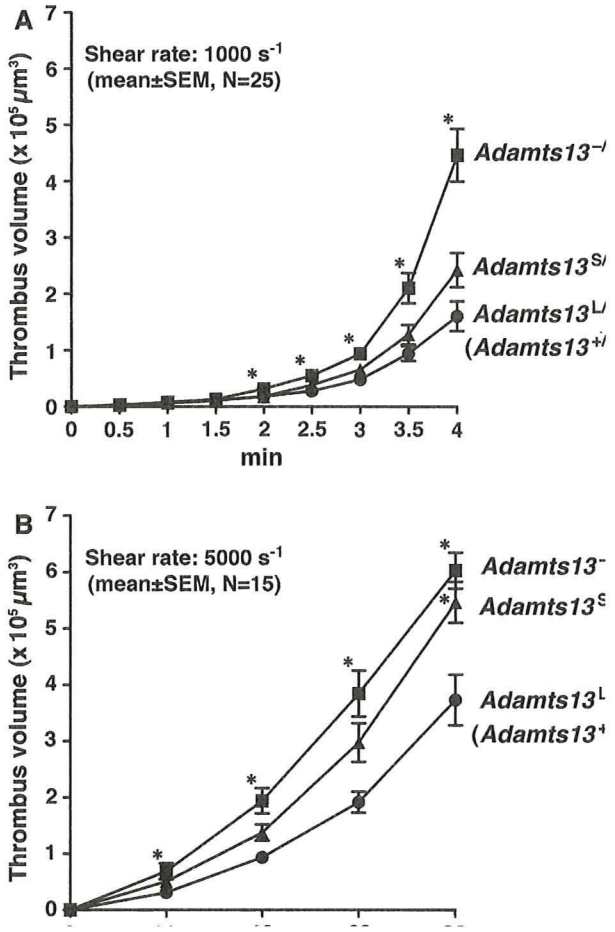

Fig. 2 Platelet thrombus formation in ADAMTS13-mutant mice on collagen surface under flow. **a** Thrombus formation at 1,000 s^{-1}. Whole blood samples from *Adamts13*$^{L/L}$ (*Adamts13*$^{+/+}$), *Adamts13*$^{S/S}$, or *Adamts13*$^{-/-}$ mice containing mepacrine-labeled platelets are perfused over an acid-insoluble type I collagen-coated surface at a wall shear rate of 1,000 s^{-1}. The cumulative thrombus volume, analyzed using a multi-dimensional imaging system, is measured every 0.5 min until 4 min. Data are the mean ± SEM of 25 mice for each genotype. **b** Thrombus formation at 5,000 s^{-1}. Whole blood samples from indicated mice are perfused over an acid-insoluble type I collagen-coated surface at a wall shear rate of 5,000 s^{-1}. The cumulative thrombus volume is measured every 20 s until 80 s. Blood from two mice is pooled and used for experiments. Data are the mean ± SEM of 15 samples for each genotype. *Asterisks* indicate significant differences at $P < 0.05$ in comparison to *Adamts13*$^{L/L}$ mice

accelerated thrombogenic responses in *Adamts13*$^{-/-}$ mice under in vitro flow conditions (Fig. 2). When whole blood is perfused over a collagen-coated surface in a parallel plate-flow chamber at wall shear rates of 750–5,000 s^{-1}, cumulative platelet thrombus volume is significantly higher in *Adamts13*$^{-/-}$ mice compared to *Adamts13*$^{+/+}$ mice [2, 4]. In vivo consequence of a lack of ADAMTS13 was further evaluated using collagen plus epinephrine infusion model experiments. In this model, widespread intravascular thrombosis is induced by intravenous infusion of collagen fibrils in combination with epinephrine, and the incorporation of platelets into thrombi is monitored by the reduction in circulating platelet counts. Following the infusion of collagen plus epinephrine, reduction of platelet counts is more severe in *Adamts13*$^{-/-}$ mice than in *Adamts13*$^{+/+}$ mice, suggesting that a complete lack of ADAMTS13 in mice results in a prothrombotic state.

Using the intravital microscopy, Motto et al. [3] have also elegantly shown prothrombotic phenotypes of *Adamts13*$^{-/-}$ mice in vivo. Upon activation of endothelial cells with secretagogues such as histamine and calcium ionophore A23187, UL-VWF multimers stored in Weibel-Palade bodies are released into circulation. It was demonstrated in vitro that quiescent platelets can rapidly bind to the UL-VWF multimers resulting in formation of long platelet strings and ADAMTS13 can cleave anchored platelet strings on the surface of endothelium [7]. Following stimulation with histamine or A23187, long-lived platelet strings ranging from 30 to 250 μm are observed only in *Adamts13*$^{-/-}$ mice. These strings remain anchored at one end and waved with another end in the blood stream [3]. In addition, following superfusion with A23187, prolonged platelet adhesion is observed in *Adamts13*$^{-/-}$ mice compared to *Adamts13*$^{+/+}$ mice. Adhesion is absent in stimulated veins of *Vwf*$^{-/-}$ mice confirming that prolonged platelet adhesion depends on VWF [3]. These results are the direct evidence that ADAMTS13 regulates VWF-mediated platelet adhesion in vivo.

After topical superfusion of A23187, spontaneous platelet aggregation resulting in microthrombi formation is observed in the microvessels (25–30 μm) of *Adamts13*$^{-/-}$ mice [8]. In *Adamts13*$^{+/+}$ mice treated identically, small platelet aggregates can be seen attached to the endothelium for 1–2 s, but thrombi do not form. When arterioles are injured by a $FeCl_3$-treatment, platelet binding to subendothelium is increased and thrombus formation is significantly accelerated in *Adamts13*$^{-/-}$ mice compared to *Adamts13*$^{+/+}$ mice [8]. In another set of $FeCl_3$-induced vessel injury in *Vwf*$^{-/-}$ mice, most of the vessels do not occlude in either mice expressing ADAMTS13 or lacking ADAMTS13, demonstrating that ADAMTS13 deficiency is not sufficient to overcome the VWF deficiency in this system [9]. These results support that ADAMTS13 down-regulates platelet adhesion and aggregation in vivo, and ADAMTS13 deficiency can provide enhanced thrombus formation at the site of vascular lesions. These findings also suggest that VWF, the only relevant substrate for ADAMTS13, is critical in this model of thrombus growth under arterial shear conditions.

4.2 TTP-like phenotypes induced by shigatoxin challenge in ADAMTS13-deficient mice on the specific genetic background

CASA/Rk strain is a wild-derived mouse strain of *Mus musculus castaneus* that exhibits plasma VWF levels 5- to

10-fold higher than C57BL/6J strain. The major genetic factor that accounts for this difference is associated with a gene modifier *Mvwf2*, corresponding to the R2657Q mutation in *Vwf* gene resulting in increased biosynthesis/secretion of VWF [10]. Additional modifier loci correlating with increased VWF levels are identified in CASA/Rk strain as *Mvwf3* on chromosome 4 and *Mvwf4* on chromosome 13 [10]. The genetic background of CASA/Rk strain has been introduced onto the C57BL/6J and 129/SvJ mixed-background *Adamts13*$^{-/-}$ mice by backcrossing with wild-type CASA mice for two generations. These mice are born in expected Mendelian distribution, however, mean platelet counts of the *Adamts13*$^{-/-}$ mice are significantly reduced compared to *Adamts13*$^{+/+}$ littermates.

When challenged with shigatoxin produced by *Shigella dysenteriae* and the *Shigatoxigenic* group of *Escherichia coli*, a subset of this *Adamts13*$^{-/-}$ mice show clinical signs of TTP including thrombocytopenia, hemolytic anemia with fragmented red blood cells, and VWF-rich thrombi in multiple organs including brain, heart and kidneys [3]. Shigatoxin is toxic to endothelial cells and known to induce hemolytic uremic syndrome (HUS) that exhibits similar clinical and pathologic findings to TTP. Shigatoxin also stimulates the release of UL-VWF multimers from human umbilical vein endothelial cells and perfused quiescent platelets immediately adhere to UL-VWF multimers, resulting in formation of platelet strings [11]. Thus, environmental factors causing endothelial activation or damage can trigger TTP in *Adamts13*$^{-/-}$ mice. Because shigatoxin challenge does not evoke TTP-like symptoms in *Adamts13*$^{-/-}$ mice on the mixed background [3], introduction of the CASA/Rk genetic background provides susceptibility to TTP in *Adamts13*$^{-/-}$ mice. Of note, there is no correlation between plasma VWF level and degree of shigatoxin-induced thrombocytopenia or mortality, suggesting that TTP-modifier genes that are not associated with plasma VWF levels may be delivered from a CASA/Rk genetic background [3].

In human, there is a large variation in the phenotypes of TTP patients with ADAMTS13 deficiency [12]. Many TTP patients with congenital ADAMTS13 deficiency have their first acute episode in the neonatal period or early infancy, but late-onset cases and asymptomatic carriers in adulthood have been reported. Patients with identical ADAMTS13 mutations but different clinical courses have been described, indicating that ADAMTS13 deficiency brings a serious risk but is not a sufficient condition for TTP. Data from *Adamts13*$^{-/-}$ mice support this view, and *Adamts13*$^{-/-}$ mice can contribute to the identification of additional genetic and/or environmental TTP triggers.

The only known substrate for ADAMTS13 is VWF. To investigate the absolute requirement of VWF in shigatoxin-induced thrombocytopenia, VWF-null allele is crossed onto the CASA/*Adamts13*$^{-/-}$ background [9]. Challenge of VWF expressing (*Vwf*$^{+/+}$ or *Vwf*$^{+/-}$) CASA/*Adamts13*$^{-/-}$ mice with shigatoxin results in thrombocytopenia and mortality. In contrast, littermate CASA/*Adamts13*$^{-/-}$ mice deficient for VWF (*Vwf*$^{-/-}$) do not result in thrombocytopenia. These results clearly demonstrate that a threshold of VWF is required for shigatoxin-induced thrombocytopenia and provide experimental evidence for the crucial role of VWF in TTP pathogenesis.

5 Thrombogenic phenotypes in congenic mice having C-terminal truncated ADAMTS13-S

The specific functions of each of the ADAMTS13 domains in the VWF-cleavage have been studied using different types of in vitro assays. These studies have shown an essential role of the N-terminal domains from the metalloprotease to the spacer domains in substrate recognition and proteolysis [1]. However, physiological significance of the remaining C-terminal Tsp1 and CUB domains was not clearly defined in vivo. Taking advantage of the presence of the spontaneous IAP-insertional mutation in the *Adamts13* gene of some laboratory mouse strains, a congenic mouse strain (*Adamts13*$^{S/S}$) that has ADAMTS13-S on 129/Sv genetic background has recently been established [4]. In this model, C57BL/6-*Adamts13* gene with IAP mutation has been applied to 129/Sv mice by ten-generation backcrossing.

Similar to wild-type 129/Sv mice (*Adamts13*$^{L/L}$), *Adamts13*$^{S/S}$ mice do not have UL-VWF multimers in plasma, in contrast to 129/Sv-genetic background ADAMTS13-deficient mice (*Adamts13*$^{-/-}$) [4]. Hence, the C-terminal domains of ADAMTS13 are not necessary for removal of UL-VWF multimers in plasma under physiological conditions. However, parallel plate flow chamber experiments show that blood from *Adamts13*$^{S/S}$ mice is more thrombogenic under flow at a high shear rate of 5,000 s^{-1} in compared to blood from *Adamts13*$^{L/L}$ mice (Fig. 2) [4]. In addition, both in vivo thrombus formation in $FeCl_3$-injured arterioles and thrombocytopenia induced by collagen plus epinephrine challenge are accelerated in *Adamts13*$^{S/S}$ mice compared to *Adamts13*$^{L/L}$ mice [4]. These results provide in vivo insights on physiological significance of the C-terminal domains of ADAMTS13 in down-regulating thrombus growth.

6 The function of ADAMTS13 in sepsis and endotoxemia

Some of the recent studies have found reduced ADAMTS13 activity in patients with acute systemic inflammation

or sepsis, suggesting a role for VWF-ADAMTS13 axis in sepsis [13]. To investigate the functions of VWF and ADAMTS13 in sepsis and endotoxemia, two different groups have done independent studies using two different models; one by LPS-induced sepsis [9] and the other by cecum ligature and puncture (CLP) in mice [14]. When $Vwf^{+/+}$ or $Vwf^{-/-}$ mice are challenged with LPS, there is no significant difference in LPS-induced thrombocytopenia or mortality up to 4 days of observation period [9]. In contrast, in CLP-induced sepsis model there is a decrease in mortality of VWF-deficient mice compared to wild-type mice, suggesting important role for VWF secretion in sepsis-induced mortality [14]. The different finding in two independent studies illustrates the importance of different models used for sepsis.

There is also no significant difference in LPS-induced mortality in VWF expressing mice that are either lacking or expressing ADAMTS13. Additionally, mice deficient for VWF and ADAMTS13 also exhibited similar thrombocytopenia and mortality. These observations in mice suggest that neither absolute VWF deficiency nor ADAMTS13 has effect on LPS-induced sepsis [9]. These findings are in agreement with the report that complete deficiency of ADAMTS13 in mice is not associated with excess mortality in CLP-induced sepsis [14]. However, they have found a decrease in ADAMTS13 activity in wild-type mice after CLP-induced sepsis, similar to that reported previously in human sepsis [13]. However, deficiency of ADAMTS13 in mouse does not modulate CLP-induced sepsis. The decrease in ADAMTS13 activity in CLP-induced sepsis is most probably due to consumption of ADAMTS13 to VWF released in large amounts.

7 The function of ADAMTS13 in inflammation

Recently, Chauhan and colleagues [15] have investigated the role of ADAMTS13 and its substrate VWF in inflammation by studying leukocyte rolling and adhesion in $Adamts13^{+/+}/Vwf^{+/+}$, $Adamts13^{-/-}/Vwf^{+/+}$, $Adamts13^{+/+}/Vwf^{-/-}$ and $Adamts13^{-/-}/Vwf^{-/-}$ mice using intravital microscopy. They have shown that ADAMTS13-deficiency in mice results in higher numbers of leukocytes rolling on the unstimulated endothelium compared to wild-type. The increase in the leukocyte rolling observed in $Adamts13^{-/-}$ mice is VWF-dependent.

There is also an increase in endothelial P-selectin expression, soluble P-selectin and VWF in plasma of $Adamts13^{-/-}$ mice. These observations raise the question how ADAMTS13 deficiency results in increased plasma VWF. One of the reasons could be that ADAMTS13 deficiency results in slower clearance of UL-VWF multimers from the circulation and thus elevated VWF levels.

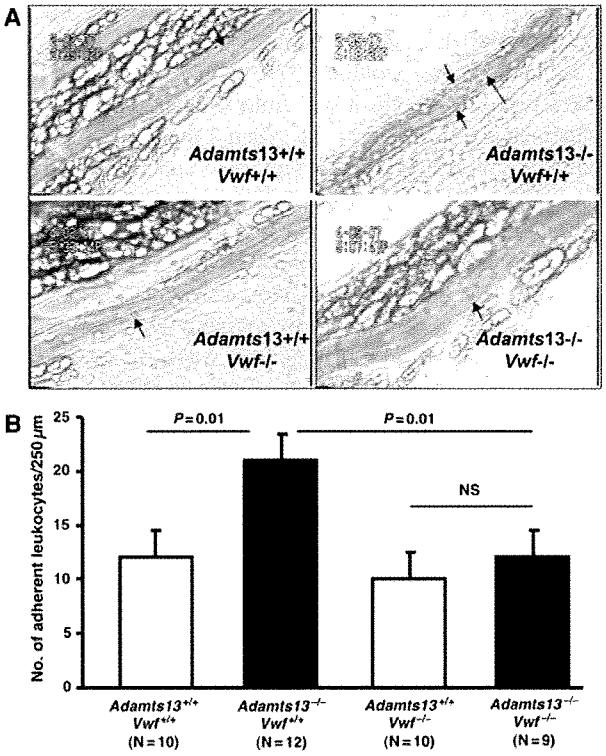

Fig. 3 Increased leukocyte adhesion in the TNF α-stimulated mesenteric venules of ADAMTS13-deficient mice. Mice are treated with the inflammatory cytokine TNF-α for 3.5 h before intravital microscopy. A single mesenteric venule (25–30 µm diameter) is studied per mouse. **a** Representative images are shown. *Arrows* indicate leukocytes adhering to inflamed endothelium. **b** Quantification of the adherent leukocytes. The number of adherent leukocytes is markedly increased in the microvenules of $Adamts13^{-/-}$ mice compared to $Adamts13^{+/+}$ mice. In contrast, the number of leukocytes adhering in venules of $Adamts13^{-/-}/Vwf^{-/-}$ mice is similar to $Adamts13^{+/+}/Vwf^{-/-}$ mice, suggesting that VWF plays a role in increased leukocyte adhesion in $Adamts13^{-/-}$ vessels. Data represent the mean ± SEM. NS, $P > 0.05$

Alternatively, UL-VWF multimers activate platelets, which in turn may activate the endothelium. Previously, it has been shown that activated platelets, by binding to leukocytes, promote Weibel-Palade bodies release and stimulate leukocyte rolling [16]. Interestingly, depletion of platelets in $Adamts13^{-/-}$ mice results in normalization of leukocyte rolling as compared to wild-type mice. This indicates that platelets, likely activated by UL-VWF either in circulation or directly on endothelium, stimulate Weibel-Palade body's secretion. Moreover, when $Adamts13^{-/-}$ mice veins are stimulated with histamine, a secretagogue of Weibel-Palade bodies, in order to release UL-VWF multimers, leukocyte rolling velocity is slower when compared to wild-type mice veins where platelet strings do not form [15]. These in vivo findings are in agreement with previous in vitro studies where it was shown that platelets bound to endothelial UL-VWF could support leukocyte tethering

and rolling and that VWF acts as a ligand for leukocyte receptors PSGL-1 and $\beta 2$ integrin [17].

Inflammatory cytokines TNF-α and IL-8 have been shown to release UL-VWF from human umbilical vein endothelial cells in vitro [18]. When *Adamts13*$^{-/-}$ mice are challenged with TNF-α, the number of adherent leukocytes increases approximately twofold in activated venules of *Adamts13*$^{-/-}$ mice when compared to wild-type mice [15]. This process is dependent on VWF (Fig. 3). In addition, ADAMTS13 deficiency in mouse results in increased extravasation of neutrophils in both thioglycollate-induced peritonitis and wound healing [15]. These in vitro and in vivo studies suggest that UL-VWF multimers released from Weibel-Palade bodies by many stimuli including hypoxia, changes in shear stress, and inflammatory cytokines could accelerate inflammatory responses in diseases such as atherosclerosis and stroke when not digested by ADAMTS13.

The results from the *Adamts13*$^{-/-}$ mice suggest that, by cleaving hyperactive UL-VWF multimers, ADAMTS13 not only down-regulates thrombosis but also inflammation. The studies reported here may provide new insights on the possible uses of ADAMTS13 as a therapeutic agent.

References

1. Banno F, Miyata T. Biology of an antithrombotic factor-ADAMTS13. In: Tanaka K, Davie EW, editors. Recent advances in thrombosis and hemostasis 2008. Springer; 2008. p. 162–76.
2. Banno F, Kokame K, Okuda T, Honda S, Miyata S, Kato H, et al. Complete deficiency in ADAMTS13 is prothrombotic, but it alone is not sufficient to cause thrombotic thrombocytopenic purpura. Blood. 2006;107:3161–6.
3. Motto DG, Chauhan AK, Zhu G, Homeister J, Lamb CB, Desch KC, et al. Shigatoxin triggers thrombotic thrombocytopenic purpura in genetically susceptible ADAMTS13-deficient mice. J Clin Invest. 2005;115:2752–61.
4. Banno F, Chauhan AK, Kokame K, Yang J, Miyata S, Wagner DD, et al. The distal carboxyl-terminal domains of ADAMTS13 are required for regulation of in vivo thrombus formation. Blood. 2009;113:5323–9.
5. Banno F, Kaminaka K, Soejima K, Kokame K, Miyata T. Identification of strain-specific variants of mouse *Adamts13* gene encoding von Willebrand factor-cleaving protease. J Biol Chem. 2004;279:30896–903.
6. Zhou W, Bouhassira EE, Tsai HM. An IAP retrotransposon in the mouse *ADAMTS13* gene creates ADAMTS13 variant proteins that are less effective in cleaving von Willebrand factor multimers. Blood. 2007;110:886–93.
7. Dong JF, Moake JL, Nolasco L, Bernardo A, Arceneaux W, Shrimpton CN, et al. ADAMTS-13 rapidly cleaves newly secreted ultralarge von Willebrand factor multimers on the endothelial surface under flowing conditions. Blood. 2002; 100:4033–9.
8. Chauhan AK, Motto DG, Lamb CB, Bergmeier W, Dockal M, Plaimauer B, et al. Systemic antithrombotic effects of ADAMTS13. J Exp Med. 2006;203:767–76.
9. Chauhan AK, Walsh MT, Zhu G, Ginsburg D, Wagner DD, Motto DG. The combined roles of ADAMTS13 and VWF in murine models of TTP, endotoxemia, and thrombosis. Blood. 2008;111:3452–7.
10. Westrick RJ, Ginsburg D. Modifier genes for disorders of thrombosis and hemostasis. J Thromb Haemost. 2009;7(Suppl 1):132–5.
11. Nolasco LH, Turner NA, Bernardo A, Tao Z, Cleary TG, Dong JF, et al. Hemolytic uremic syndrome-associated Shiga toxins promote endothelial-cell secretion and impair ADAMTS13 cleavage of unusually large von Willebrand factor multimers. Blood. 2005;106:4199–209.
12. Lämmle B, Kremer Hovinga JA, Alberio L. Thrombotic thrombocytopenic purpura. J Thromb Haemost. 2005;3:1663–75.
13. Martin K, Borgel D, Lerolle N, Feys HB, Trinquart L, Vanhoorelbeke K, et al. Decreased ADAMTS-13 (A disintegrin-like and metalloprotease with thrombospondin type 1 repeats) is associated with a poor prognosis in sepsis-induced organ failure. Crit Care Med. 2007;35:2375–82.
14. Lerolle N, Dunois-Larde C, Badirou I, Motto DG, Hill G, Bruneval P, et al. von Willebrand factor is a major determinant of ADAMTS-13 decrease during mouse sepsis induced by cecum ligation and puncture. J Thromb Haemost. 2009;7:843–50.
15. Chauhan AK, Kisucka J, Brill A, Walsh MT, Scheiflinger F, Wagner DD. ADAMTS13: a new link between thrombosis and inflammation. J Exp Med. 2008;205:2065–74.
16. Dole VS, Bergmeier W, Mitchell HA, Eichenberger SC, Wagner DD. Activated platelets induce Weibel-Palade-body secretion and leukocyte rolling in vivo: role of P-selectin. Blood. 2005; 106:2334–9.
17. Pendu R, Terraube V, Christophe OD, Gahmberg CG, de Groot PG, Lenting PJ, et al. P-selectin glycoprotein ligand 1 and beta2-integrins cooperate in the adhesion of leukocytes to von Willebrand factor. Blood. 2006;108:3746–52.
18. Bernardo A, Ball C, Nolasco L, Moake JF, Dong JF. Effects of inflammatory cytokines on the release and cleavage of the endothelial cell-derived ultralarge von Willebrand factor multimers under flow. Blood. 2004;104:100–6.

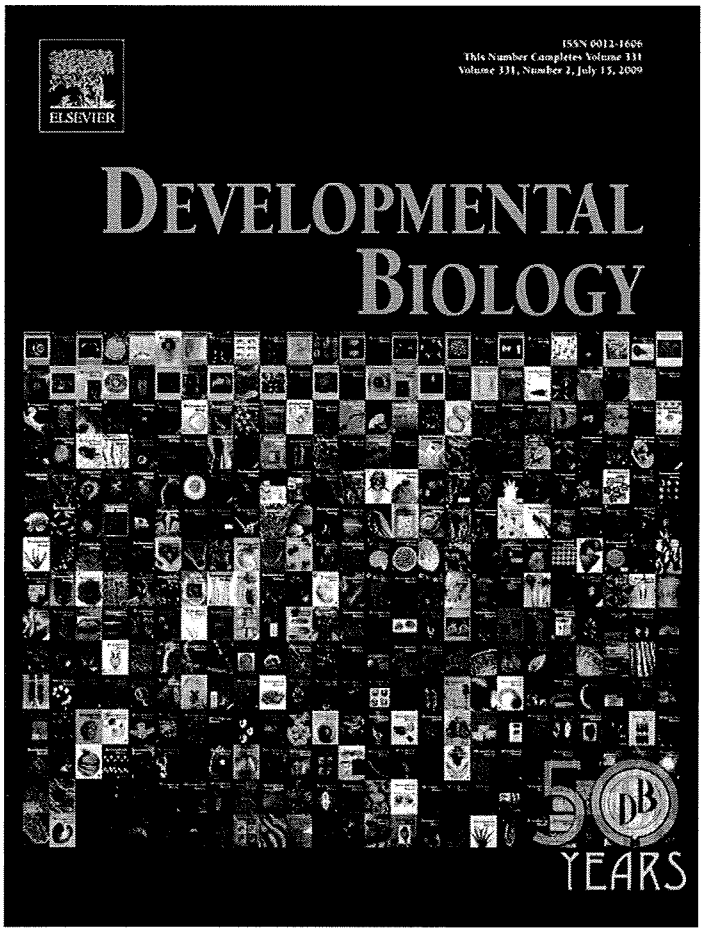

Developmental Biology 331 (2009) 140–151

Contents lists available at ScienceDirect

Developmental Biology

journal homepage: www.elsevier.com/developmentalbiology

The transcriptional repressor RP58 is crucial for cell-division patterning and neuronal survival in the developing cortex

Haruo Okado [a,*,1,2,3], Chiaki Ohtaka-Maruyama [a,1,2,4], Yoshinobu Sugitani [b,1,2,4], Yuko Fukuda [c,2], Reiko Ishida [c,2], Shinobu Hirai [a,2], Akiko Miwa [a,2], Akiyo Takahashi [a,2], Katsunori Aoki [d,2], Keiji Mochida [e,2,4], Osamu Suzuki [f,4], Takao Honda [g,2], Kazunori Nakajima [g,4], Masaharu Ogawa [b,4], Toshio Terashima [h,4], Junichiro Matsuda [f,2,5], Hitoshi Kawano [i,1,4], Masataka Kasai [c,1]

[a] Department of Molecular Physiology, Tokyo Metropolitan Institute for Neuroscience, 2-6 Musashidai, Fuchu, Tokyo 183-8526, Japan
[b] Ogawa research unit, Neuro-developmental disorder research group, Brain Science Institute, Riken, Saitama 351-0198, Japan
[c] Department of Immunology, National Institute of Infectious Diseases, 1-23-1 Toyama, Shinjuku-ku, Tokyo 162-8640, Japan
[d] Department of Hematology (Internal Medicine), The University of Tokyo, Bunkyo-ku, Tokyo 113-8655, Japan
[e] Bioresource Center, RIKEN, Tsukuba, Ibaraki 305-0074, Japan
[f] Department of Veterinary Science, National Institute of Infectious Diseases, 1-23-1 Toyama, Shinjuku-ku, Tokyo 162-8640, Japan
[g] Department of Anatomy, Keio University School of Medicine, Tokyo 160-8582, Japan
[h] Division of Anatomy and Developmental Neurobiology, Department of Neuroscience, Kobe University Graduate School of Medicine, Kobe 650-0017, Japan
[i] Department of Developmental Morphology, Tokyo Metropolitan Institute for Neuroscience, 2-6 Musashidai, Fuchu, Tokyo 183-8526, Japan

ARTICLE INFO

Article history:
Received for publication 23 August 2008
Revised 1 April 2009
Accepted 24 April 2009
Available online 3 May 2009

Keywords:
RP58
Transcriptional repressor
Cerebral cortex
Apoptosis
Cell-cycle exit
Progenitor cell

ABSTRACT

The neocortex and the hippocampus comprise several specific layers containing distinct neurons that originate from progenitors at specific development times, under the control of an adequate cell-division patterning mechanism. Although many molecules are known to regulate this cell-division patterning process, its details are not well understood. Here, we show that, in the developing cerebral cortex, the RP58 transcription repressor protein was expressed both in postmitotic glutamatergic projection neurons and in their progenitor cells, but not in GABAergic interneurons. Targeted deletion of the *RP58* gene led to dysplasia of the neocortex and of the hippocampus, reduction of the number of mature cortical neurons, and defects of laminar organization, which reflect abnormal neuronal migration within the cortical plate. We demonstrate an impairment of the cell-division patterning during the late embryonic stage and an enhancement of apoptosis of the postmitotic neurons in the *RP58*-deficient cortex. These results suggest that RP58 controls cell division of progenitor cells and regulates the survival of postmitotic cortical neurons.

Introduction

Glutamatergic cortical neurons are generated from progenitor cells in the cortical germinal zone and migrate radially in an inside-to-outside gradient. The earliest neurons form the preplate (together with the Cajal-Retzius cells) and the neurons born subsequently migrate past the earliest-born neurons to intercalate within the preplate, divide it into the marginal zone (MZ; layer 1) and the subplate (layer 6b), and form the lower layers of the cortical plate (CP). Late-born neurons then migrate past the early-born neurons to form the upper layers of the CP, beneath the MZ. In contrast, GABAergic neurons and Cajal-Retzius cells are generated from progenitor cells outside the neocortex, in the ganglion eminence and in the cortical hem, respectively, and migrate tangentially into the neocortex (Bayer and Altman, 1991; Allendoerfer and Shatz, 1994; Molyneaux et al., 2007). The radial glial progenitors (RGPs) in the ventricular zone (VZ) give rise to cortical neurons, while the progenitor cells in the subventricular zone (SVZ) produce a substantial number of upper-layer neurons (Smart and McSherry, 1982, Tarabykin et al., 2001, Sugitani et al., 2002). Some of the SVZ progenitor cells are intermediate progenitors (IMPs), which originate from the VZ and produce neurons by dividing limited times (Noctor et al., 2004; Haubensak et al., 2004; Miyata et al., 2004). In the hippocampus, pyramidal neurons of the Cornu Ammonis (CA) are generated from the VZ of the hippocampus, whereas the precursors of the granular neurons of the dentate gyrus (DG) originate in the neuroepithelium near the cortical hem, migrate towards the anlage of

* Corresponding author.
E-mail address: hokado@tmin.ac.jp (H. Okado).
[1] H.O, C.O-M, Y.S, H.K. and M.K. designed the research.
[2] H.O, C.O-M, Y.S., Y.F., R.I., S.H., A.M., A.T., K.A., K.M., T.H., J.M. performed the research.
[3] H.O. wrote the paper.
[4] C.O-M, Y.S., O.S., K.N., M.O. T.T., H.K., K.M. provided helpful discussion and guidance.
[5] Present address: National Institute of Biomedical Innovation, Ibaraki City, Osaka 567-0085, Japan.

0012-1606/$ – see front matter © 2009 Elsevier Inc. All rights reserved.
doi:10.1016/j.ydbio.2009.04.030

the DG, continue to divide, and undergo further migration to the granule layer of the DG (Forster et al., 2006; Li and Pleasure 2007).

These cortical progenitor cells generate a vast diversity of terminally differentiated neuronal phenotypes. The balance between exit from and reentry into the cell cycle is important for the formation of these cell types at appropriate times; however, the molecular mechanism underlying this regulation is not completely understood (Dehay and Kennedy, 2007).

We have previously described a novel DNA binding protein, RP58 (also known as ZNF238), which shares homology with the POZ domain of a number of zinc finger (ZF) proteins, which are termed POZ-ZF proteins (Aoki et al., 1998). RP58 exhibits a sequence-specific transcriptional repressor activity (Aoki et al., 1998) and probably acts by binding to the DNA methyltransferase Dnmt3a, which associates with histone deacetylase and acts as a corepressor (Fuks et al., 2001). POZ-ZFs are important for many biological processes, which include B-cell fate determination, DNA damage responses, cell-cycle progression, and a multitude of developmental events (Kelly and Daniel, 2006). Among the POZ-ZF proteins, the promyelocytic leukemia zinc finger (PLZF) is essential for stem cell self renewal in the murine testis (Buaas et al., 2004; Costoya et al. 2004), Miz1 plays an essential role in the control of the exit from the cell cycle during the hair cycle (Gebhardt et al., 2007), and ZENON is involved in the maintenance of panneuronal features and/or in the survival of mature neurons (Kiefer et al., 2005).

We demonstrated that RP58 transcripts are highly expressed in the cerebral cortex in the embryonic mouse brain (Ohtaka-Maruyama et al., 2007). In addition, RP58 is expressed weakly in the VZ and intensely in the SVZ, intermediate zone (IZ), and CP in the embryonic cortex, which suggests that RP58 is important for the early development of cortical neurons. In adult cerebral cortex, the expression of the RP58 transcript is maintained in glutamatergic neurons, but not in GABAergic neurons.

In the present study, we investigated the role of RP58 in the development of the cerebral cortex by generating and analyzing *RP58*-deficient mice. Our results demonstrate that *RP58* deficiency causes enhanced apoptosis and impairs the cell-division patterning in the VZ during late development, which suggests that RP58 is a novel regulator of glutamatergic neuron survival and of progenitor cell division.

Materials and methods

Generation of RP58-deficient mice

Similarly to what is observed for the human *RP58* gene, the sequence of the mouse *RP58* gene that encodes the functional protein is uninterrupted over its entire 4.2 kb length (Meng et al., 2000). A gene-targeting construct was prepared by deletion of the entire exon (5.4 kb). The resulting *RP58* targeting vector (Supplementary Fig. 1A), which was constructed from a mouse strain 129 library (Stratagene) and consisted of a 4.2 kb homology arm derived from the 5' end of the exon, a PGK promoter-neomycin expression cassette, and a 2.7 kb homology arm from the 3' end of the exon, was linearized with XbaI and introduced into GSI ES cells (derived from the 129/SvJ mouse strain) by electroporation. Colonies that survived after selection were picked and expanded for DNA analysis. Targeted ES cells were injected into the blastocoel cavity of C57/BL6 embryos using a piezo-driven micromanipulator (PrimeTech, Tsuchiura, Japan) to generate chimeric mice, which were then crossed with C57/BL6 females to obtain heterozygous $RP58^{+/-}$ mutant animals. These mice were, in turn, interbred to produce homozygous $RP58^{-/-}$ mice at the expected Mendelian frequency.

Southern blot analysis of genomic DNA isolated from the tails of embryonic day (E) 18.5 fetuses confirmed the homologous integration of the target vector (Supplementary Fig. 1B), which resulted in the replacement of the entire *RP58* exon (5.4 kb) with the neomycin resistance gene. Northern blot analysis of total RNA extracted from genotyped embryonic brains (Supplementary Fig. 1C) showed that the RP58 transcript was present only in wild-type and heterozygous embryos. In homozygous mutant embryos, no RP58 transcript of any size was observed. Embryonic brain extracts were incubated with anti-RP58-conjugated Sepharose 4B beads. The beads were washed extensively and boiled in SDS sample buffer. After centrifugation, the supernatant was analyzed for the presence of RP58 by immunoblotting, as described previously (Ishida et al., 2002). To confirm the specificity of the interactions between the antigen and the antibody, the peptide (CLPTVRDWTLEDSSQELWK) used for the generation of the anti-RP58 antibody was added during the immunoprecipitation experiment. Antibodies specific to RP58 detected the protein in brain extracts from wild-type, but not homozygous mutant, embryos (Supplementary Fig. 1D). The day after the mating was designated E0.5.

Immunohistochemistry

Heads of embryos were removed, fixed in Bodian's fixative (3.7% formaldehyde, 80% ethanol), embedded in paraffin, and sectioned at an 8 μm thickness. A few embryos were perfused with 4% paraformaldehyde and sectioned using a cryostat (10–25 μm thickness). In most cases, the antigens in these sections were reactivated by heating in 10 mM citrate buffer (adjusted to pH 6.0) using a microwave or an autoclave.

We used the following antibodies: rabbit anti-mouse RP58 (1:500, Takahashi et al., 2008), mouse anti-reelin (1:200, Chemicon), rabbit anti-MAP2 (1:500, Chemicon), rabbit anti-Tbr1 (1:500, Chemicon), rabbit anti-Prox1 (1:1000, Covance), chicken anti-Tuj1 (1:200, Chemicon), mouse anti-BrdU (1:50, Becton-Dickinson), rat anti-BrdU (1:200, Abcam), mouse anti-α-synuclein, mouse anti-β-synuclein (1:200, BD Transduction Lab), rabbit anti-Pax6 (1:200, Chemicon), mouse anti-PCNA (1:200, Chemicon), mouse anti-nestin (1:200, Rat-401), mouse anti-NeuN (1:100, Chemicon), mouse anti-Ki67 (1:100, Novocastra), rabbit anti-Ki67 (1:500, Novocastra), goat anti-NeuroD (1:100, Santa Cruz Biotechnology), guinea pig anti-Dlx2 (1:1000, gift from Dr. Yoshikawa; Kuwajima et al., 2006), mouse anti-Neurogenin2 (1:5, gift from Dr. Anderson), rabbit anti-phosphohistone H3 (P-H3) (1: 200, Upstate), rabbit anti-neurofilament (1:500, Fukuda et al., 1997), rabbit anti-ssDNA (1:400, DAKO), rabbit anti-active caspase 3 (1:400, R&D), and goat anti-Unc5d (1:200, R&D).

Anti-IgG antibodies conjugated to biotin (Vector, 1:200), Alexa 488, Alexa 546, Alexa 555, Cy3, or Cy5 (1:500) (Molecular Probes or Jackson Laboratories) were used as secondary antibodies and the ABC kit (Vector) or the TSA Fluorescence System (PerkinElmer) were used to detect biotin. After nuclear staining with DAPI and Topro3, the sections were mounted with PermaFluor (Immunon) or were dehydrated and mounted with Entellan Neu (Merk). A laser-scanning confocal microscope was used to image fluorescence signals.

To perform RP58/Pax6 and RP58/Tbr2 double labeling using rabbit polyclonal antibodies, we used the TSA or TSA Plus Fluorescence System (PerkinElmer), according to Friocourt et al. (2008). Sections were first incubated with diluted anti-RP58 antibody (1:8000), for the TSA Plus Fluorescence System, and were then incubated with rabbit anti-Pax6 antibody (1:200), anti-Tbr2 antibody (1:200), or no antibody (negative control). For RP58/P-H3 double labeling, sections were first incubated with anti-RP58 antibody (1:500), for the TSA Fluorescence System, and were then incubated with rabbit anti-P-H3 antibody (1:200). For Pax6/Tbr2 double labeling, sections were first incubated with diluted anti-Pax6 antibody (1:30000), for the TSA Plus Fluorescence System, and were then incubated with rabbit anti-Tbr2 antibody (1:200). For Pax6/Tbr2/Unc6d triple labeling, sections were first incubated with diluted anti-Pax6 antibody (1:15000), for the TSA Plus Fluorescence System, and were then incubated with rabbit anti-Tbr2 (1:200) and anti-Uncd5 (1:200) antibodies.

RNA in situ hybridization

We used single-stranded digoxigenin (DIG)-UTP-labeled RNA probes generated from the mouse *RP58* cDNA (approximately 1.6 kb); mouse *ER81* (a gift from Dr. Jessell; Arber et al., 2003); mouse *RORβ* (a gift from Dr. McConnell; Weimann et al., 1999); *Svet1* (a gift from Dr. Tarabykin; Tarabykin et al., 2001); *NT3* (a gift from Dr. Aizawa; Shinozaki et al., 2004); rat *SCIP* (a gift from Dr. Lemke), mouse α-crystalline (a gift from Dr. Funatsu; Funatsu et al., 2004), rat *KA1* (a gift from Dr. Boulter; Better et al., 1990), for mouse *Tbr1*, mouse *mSorLA*; mouse *CTGF*, and mouse *Tailless* (gifts from Drs. Y Sugitani and T Noda; Sugitani et al., 2002); *HES5* cDNA (a gift from Dr. Guillemot; Cau et al., 2000). Some probes were hydrolyzed to a length of about 200–500 bp. RNA *in situ* hybridization was performed on Bodian's-fixed paraffin sections, according to the method of Ohtaka-Maruyama et al. (2007), and on 4% paraformaldehyde-fixed frozen sections, according to the method of Sugitani et al. (2002). In some cases, the counterstaining was performed using Nuclear Fast Red (Kernechtrot).

BrdU- and IdU-labeling experiments

Bromodeoxyuridine (BrdU) or iododeoxyuridine (IdU) (50 mg/kg of body weight) were injected intraperitoneally into pregnant mice at various developmental stages. To estimate the rates of cell-cycle exit, randomly selected BrdU-positive cells (about 50 cells) were examined for PCNA or Pax6 immunoreactivity 24 h after the incorporation of BrdU. In particular, the rates of cell-cycle exit were estimated in the lower region (which corresponded to the VZ) and in the upper region (which corresponded to the SVZ and IZ) of E16.5 embryos in which BrdU was incorporated on E15.5. The total number of BrdU-positive cells was counted and examined for Pax6 immunoreactivity (which corresponds to 0.09 mm of the ventricular surface). The SVZ was identified by staining with Unc5d/Svet1.

To estimate the production of progenitor cells, randomly selected Ki67-positive cells were examined for BrdU immunoreactivity 0.5 h after the incorporation of BrdU.

The estimation of cell-cycle kinetics was performed according to Martynoga et al. (2005). P_{cells} was estimated by counting the total number of cells in the prospective VZ within the sampling area.

TUNEL assay

Apoptosis was detected using a TUNEL assay kit (Dead End Fluorometric TUNEL system, Promega). Deparaffinized sections were treated with proteinase K (20 μg/ml) in 100 mM Tris–Cl and 50 mM EDTA (pH = 8.0) for 15 min at room temperature (RT), followed by treatment with FITC-nucleotide containing TdT or H_2O (as a negative control), and counterstaining using propidium iodide.

Results

Targeted disruption of the RP58 gene

To study the role of RP58 in the development of the central nervous system, we disrupted the *RP58* gene in embryonic stem cells using the target vector (see Supplementary Fig. 1A and "Materials and methods" section). Heterozygous ($RP58^{+/-}$) mice were phenotypically indistinguishable from their wild-type littermates, whereas all homozygous ($RP58^{-/-}$) mice, which were generated from intercrosses of the heterozygotes, died shortly after birth. The cause of the death remains unknown and is currently under investigation.

Hypoplasia of the hippocampus and neocortex in RP58-deficient mice

Because RP58 transcripts are expressed abundantly in the brain of the wild-type mice ($RP58^{+/+}$; Ohtaka-Maruyama et al., 2007) and $RP58^{-/-}$ mice die shortly after birth, we performed histological analyses of brains isolated from null, heterozygous, and wild-type animals at neonatal and embryonic stages. We observed hypoplasia of the neocortex and hippocampus in $RP58^{-/-}$ mice, whereas the brains of $RP58^{+/-}$ mice appeared to be normal (Fig. 1; Supplementary Figs. 1E–M). Therefore, we compared $RP58^{-/-}$ mice with either wild-type or $RP58^{+/-}$ mice in subsequent experiments. The neocortex of $RP58^{-/-}$ mice displayed a reduced thickness and its layers were disorganized. Furthermore, the VZ appeared to expand radially in the mutant cortex (asterisk in Fig. 1). In the mutant hippocampus, the pyramidal cell layer and the typical V-shaped granule cell layer of the DG were not evident (Fig. 1). Additionally, the cerebellum of $RP58^{-/-}$ mice lacked the typical foliation observed in wild-type and heterozygous animals (see Supplementary Figs. 1K–M). In the present study, we focused our analysis on the neocortex and hippocampus of mutant mice.

Reduced numbers of mature neurons in the mutant neocortex and hippocampus

Double staining of the neocortex with MAP2 and β-III-Tubulin (Tuj1) showed that postmitotic neurons were present in the mutant neocortex; however, the subplate layer was incompletely formed in the medial region of the mutant neocortex (arrowheads in Supplementary Figs. 2A–B").

To further characterize this abnormality of the neocortex, we examined the expression of various layer markers. The number of E19 subplate neurons positive for the connective tissue growth factor (CTGF), which labels maturing subplate neurons in layer 6b (Friedrichsen et al., 2003; Heuer et al., 2003), was drastically decreased in the mutant neocortex when compared with the wild type (Figs. 2A and B). To detect the subplate neurons at the earlier stage, we examined the staining for β-synuclein, which is an inhibitor

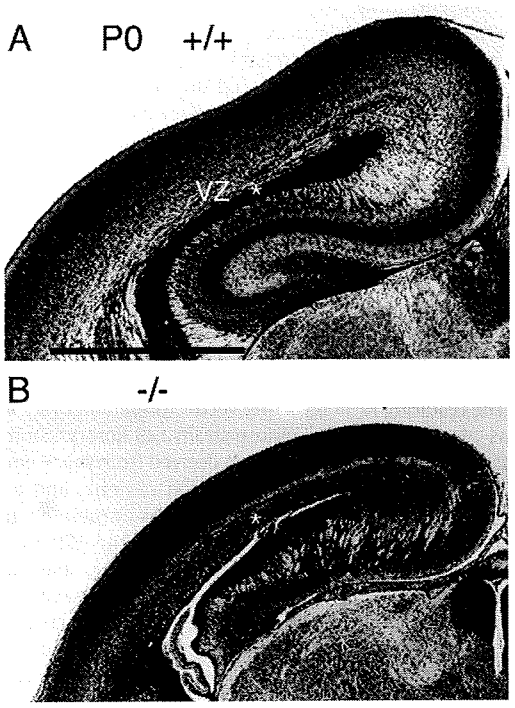

Fig. 1. Defects in brain formation in $RP58^{-/-}$ mice at P0. Nissl-stained coronal sections of forebrains from (A) wild-type (+/+) and (B) *RP58*-deficient (−/−) mice showed cytoarchitectural abnormalities in the neocortex and hippocampus of the mutant animal. In the mutant, the thickness of the neocortex was reduced and the ventricular zone (VZ) (marked with an asterisk) was expanded. Cresyl violet staining. Scale bar, 1 mm (A, B).

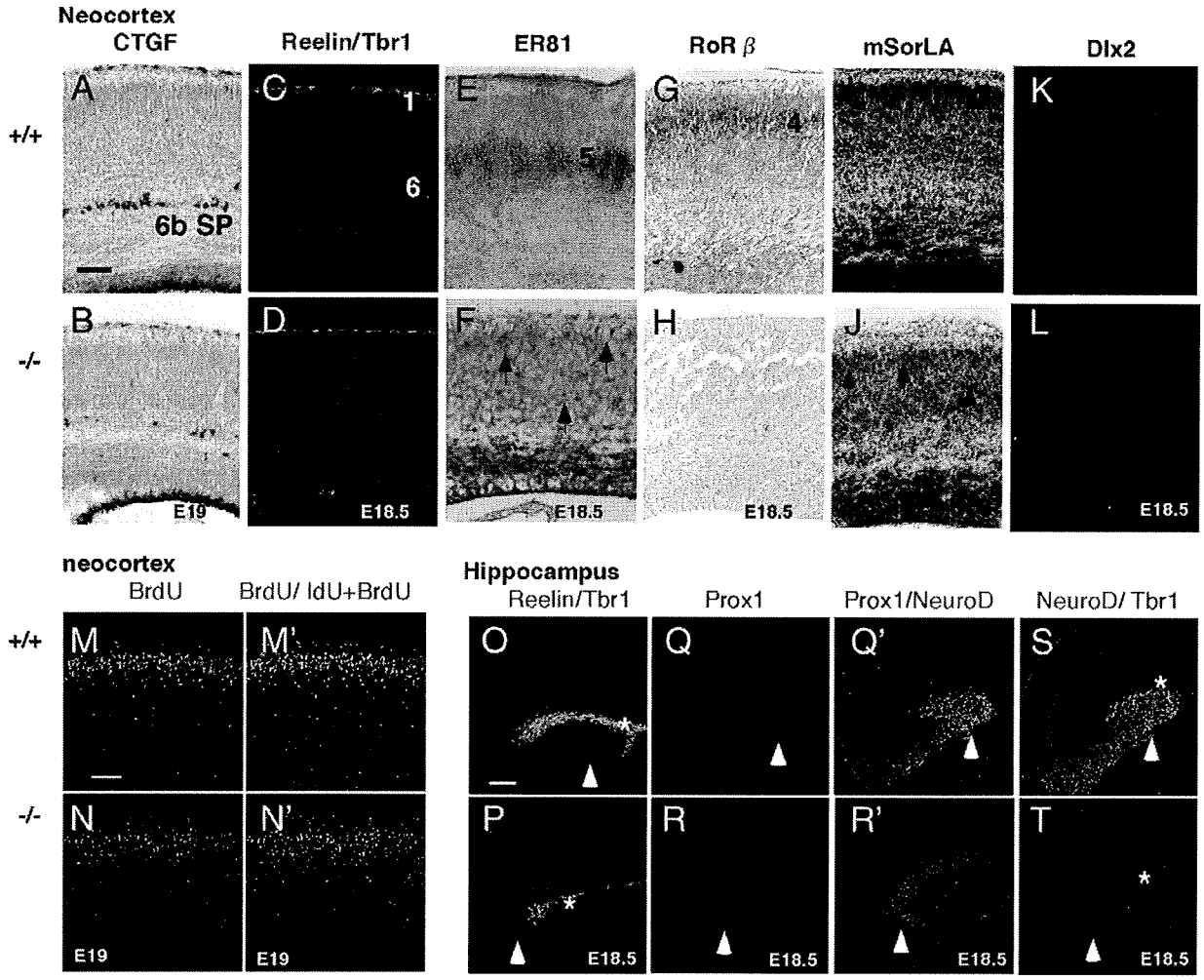

Fig. 2. Dysplasia of the neocortex and hippocampus in *RP58*$^{-/-}$ mice. (A–L) The disorganized laminar structures of the neocortex and hippocampus of the mutant were demonstrated by various layer-specific markers at E19 (A and B) or E18.5 (C–L) in the wild-type (+/+) and *RP58*-deficient (−/−) neocortex. (A and B) CTGF-labeled subplate neurons, (C and D) reelin-labeled layer 1 Cajal-Retzius neurons and Tbr1-labeled layer 6 cortical neurons, (E and F) ER81-labeled layer 5 cortical neurons, (G and H) *RoR*β-labeled layer 4 cortical neurons, (I and J) mSorLA-labeled layer 2/3 cortical neurons, and (K and L) Dlx2-labeled GABAergic neurons. In the mutant neocortex, the subplate neurons were sharply reduced in number (A and B), Cajal-Retzius neurons were normal (C and D), Tbr1-positive cells were shifted more superficially and were more widely scattered when compared with the wild type (C and D), ER81- and mSorLA-positive cells were located diffusely and in reduced numbers (arrows in F and J), the expression level of *RoR*β was dramatically reduced (G and H), and Dlx1-positive cells were roughly normal (K and L). Scale bar, 0.1 mm (A–L).

of the aggregation of α-synuclein (Hashimoto et al. 2001), as a marker for subplate neurons. Since β-synuclein is mostly detected in the deepest region of layer 6, identified with Tbr1 immunoreactivity, β-synuclein-positive cells correspond to the subplate neurons in the wild-type cortex at E16.5 (arrows in Supplementary Figs. 2E–E"). In mutant neocortices, the number of subplate neurons was severely reduced and a part of the surviving subplate neurons was displaced superficially at E16.5 (Supplementary Figs. 2C–F). In addition, in the *RP58* mutants, a fraction of the neurofilament-positive thalamocortical fibers (Kawano et al., 1999), which use subplate neurons for their pathfinding, abnormally projected towards the surface of the neocortex (Fig. 3).

Reelin-positive Cajal-Retzius neurons (Ogawa et al., 1995) developed normally in layer 1 in the E18.5 mutant (Figs. 2C and D, green). In the E18.5 mutant cortex, the majority of the Tbr1-positive cells was located in the deeper part of cortical plate (Fig. 2C; Supplementary Fig. 4E); however, many of these cells were also detected diffusely throughout the CP (Fig. 2D; Supplementary Fig. 3F). ER81, which is a layer 5 marker (Sugitani et al., 2002), was expressed in many cells in the wild-type CP (Fig. 2E); in contrast, this marker was expressed in only a few cells in the E18.5 mutant CP (arrows in Fig. 2F). Cells in the mutant cortex were only faint positive for *ROR*β, which labels layer 4 neurons (Weimann et al., 1999) (Figs. 2G and H). mSorLA labels layer 2/3 neurons (Fig. 2I, Sugitani et al., 2002; Hermans-Borgmeyer et al., 1998); mSorLA-positive cells in the mutant cortex were diffusely distributed and dramatically reduced in number (arrows in Fig. 2J). In contrast, GABA-positive (data not shown) and Dlx2-positive (Figs. 2K and L) inhibitory interneurons of the mutant neocortex did not display any distinct abnormalities, although their distribution pattern appeared slightly disturbed. These results suggest that mature subplate neurons and mature CP neurons, which form the future cortical layers 2–5, were reduced in number in *RP58*$^{-/-}$ mice.

The diffuse distribution of Tbr1-positive and other cortical neurons in the mutant cortex raised the possibility that the *RP58* deficiency impaired the inside-out layer formation. To examine this possibility, we performed double labeling by injecting iododeoxyuridine (IdU) at E12.5 and 5-bromo-2-deoxyuridine (BrdU) at E14.5, followed by examination of the brains at E19 (Figs. 2M–N'). Most late-born cortical neurons (Figs. 2M' and N', yellow) crossed over early-born cells (Figs. 2M' and N', red) in the wild-type cortex, while many late-born neurons were abnormally located beneath early-born cells in the mutant cortex. The defects of laminar organization observed in the

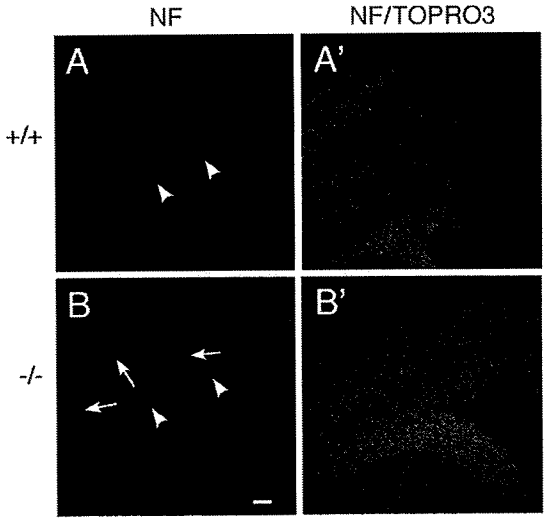

Fig. 3. Abnormality of the thalamocortical pathway formation in the *RP58*-deficent cortex. Coronal sections from E18.5 wild-type (A, A') and *RP58*$^{-/-}$ (B, B') brains stained with anti-neurofilament (NF) antibodies and TOPRO3 (nuclear stain) (A', B'). In the wild type, thalamocortical axons that were immunoreactive for neurofilament ran along the subplate beneath the cortical plate (arrowheads in A), while in the *RP58*$^{-/-}$ brain, some labeled axons ran along the subplate beneath the cortical plate (arrowheads in B), whereas the other axons invaded the cortical plate towards the pial surface (arrows in B). Scale bar, 0.1 mm (A–B').

RP58 mutant cortices suggest that RP58 may play a role in neuronal positioning or migration.

The *RP58*-deficient hippocampus was reduced in size and had no identifiable CA pyramidal layer or DG granular layer in sections stained with Nissl (Fig. 1), NeuN (Supplementary Figs. 2G' and H'), or MAP2 and Tuj1 double stain (see Supplementary Figs. 2A–B").

Cajal-Retzius cells play an important role in the normal layer formation of the hippocampus. The Tbr1/reelin double staining revealed that Cajal-Retzius cells (Nakajima et al., 1997), some of which were Tbr1-positive, were present in the mutant (Fig. 2P). The hippocampal fissure, which is characterized by Reelin-positive cells, was poorly developed (asterisk in Figs. 2O and P). In the developing p73$^{-/-}$ hippocampus, the most striking abnormality is the absence of the hippocampal fissure, which suggests a role for p73 in cortical folding (Meyer et al., 2004). Therefore, p73 and Reelin expression were examined at the cortical hem (see Supplementary Fig. 4), which revealed that the expression of p73 and reelin was both normal in *RP58*-deficient cortical hem. We next examined the CA and DG. The pan-hippocampal plate marker, α-crystalline (Funatsu et al., 2004), was expressed in a more dorsal cortical region in the mutant than in the wild type (arrows in Figs. 4A and E). Since α-crystalline is also expressed in the neocortex as well as in the hippocampus, we used another hippocampal marker, α-synuclein, together with the DG marker, Prox1. We found that α-synuclein was expressed in the hippocampal region and its staining did not overlap with the Prox1-positive region in the wild-type brain. In contrast, although α-synuclein expression was detected in the more dorsal cortical region in the mutant brain, it did not overlap with the Prox1-positive dentate region (see Supplementary Figs. 5A–B'"). These results suggested that the hippocampus was formed in a more dorsal region in the mutant, probably because of an insufficiency in hippocampal folding; however, the basic positional relationship between the CA and DG remained intact.

Furthermore, we examined whether specific hippocampal subfields were generated in the *RP58*-deficient mice. The expression of the CA3-specific marker KA1 (Grik4) (Bettler et al., 1990) was almost undetectable (an arrow in Figs. 4B and F). The CA1-specific marker SCIP (Pou3f1) (Frantz et al., 1994; arrows in Fig. 3C) was not detected (Fig. 4G). NT3, which is expressed in the cingulate neopallium (Friedman et al., 1991; Lee et al., 2000; an arrow in Fig. 4D), was also not detected in the mutant (Fig. 4H). To examine the DG, we used Prox1 and NeuroD (Figs. 2Q–T), which are markers of immature dentate granule cells (Pleasure et al., 2000; Galichet et al., 2008). In the wild type, Prox1- and NeuroD-positive cells formed a V-shaped structure, which is typical of the DG, whereas in the mutant they formed an inverted V-shaped structure (arrowhead in Figs. 2Q–T). The DG region that was positive for Prox1 appeared to extend throughout the *RP58* mutant hippocampus (Supplementary Fig. 6), suggesting that loss of RP58 function may result in an increase in the number of Prox1-positive dentate granule cells. It is reported that Tbr1 is expressed after onset of NeuroD expression (Hevner et al., 2006). Tbr1 was expressed in many NeuroD-positive dentate granule cells in the wild type, whereas its expression was severely reduced in the mutant (Figs. 2S and T), suggesting that the production of mature neurons is impaired in the mutant dentate granule cells. These results suggest that, although major areas of the hippocampus were probably retained in the mutant, the CA1, CA3 fields, the cingulate cortex, and DG were not, indicating that the hippocampal neurons had maturation defects like those seen in the neocortex.

Expression pattern of RP58 protein

The abnormality of neurons generated in the mutant cortex indicates that RP58 functions during the development of the neocortex

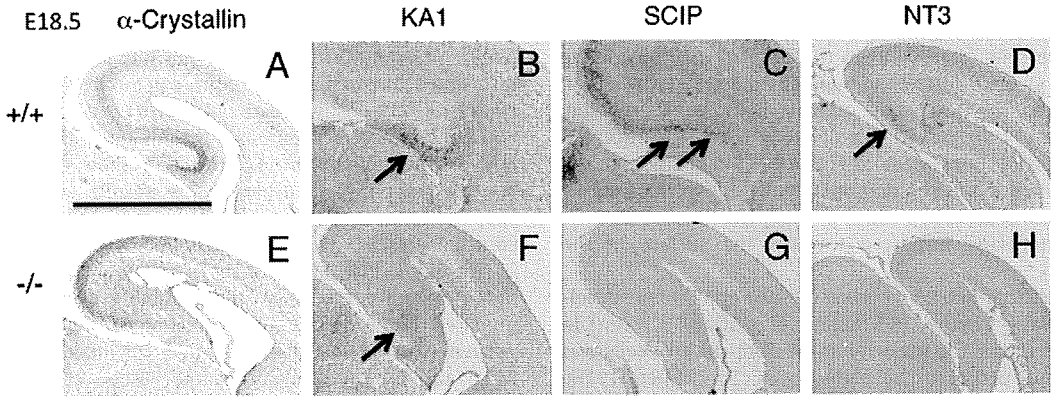

Fig. 4. Field specification impairment in the hippocampus of *RP58*-deficient E18.5 mice. α-crystalline, which is a pan-hippocampal marker, was detected in the hippocampal region of the wild-type brain (arrows in A), whereas it was detected in the more dorsal region in the *RP58*-deficient brain (arrows in E). The expression of the CA3-specific marker KA1 (an arrow in B) was almost not detected in the mutant brain (an arrow in F). In the wild-type brain, SCIP was expressed in CA1 sector of the hippocampus (arrows in C) and in the adjacent cortex, while it was not detected in the mutant brain (G). NT3, which is a cingulate neopallium marker (an arrow in D), was not detected in the mutant (H). Scale bar, 1 mm (A–H).

and of the hippocampus. To further understand the function of RP58, we examined the expression patterns of the RP58 protein using an RP58-specifc antibody (Takahashi et al., 2008). The immunostaining pattern obtained was almost identical to that of the RP58 mRNA *in situ* hybridization pattern (Figs. 5A and B). The specificity of the RP58 antibody was confirmed by immunostaining of an *RP58*$^{-/-}$ brain (Fig. 5C). Double staining using the nuclear marker TOPR3 showed that RP58 was localized in the nucleus and that it was absent from the cytoplasm (Supplementary Figs. 7B and B'''). At E12.5, RP58 was detected in preplate neurons and in some cells in the VZ (arrows in Fig. 5D). At E16.5, RP58 was present in the CP, IZ, SVZ, and in some cells in the VZ (arrows in Figs. 5E and E'), but not in cells of the MZ (Fig. 5E). Double staining with β-synuclein or Reelin indicated that RP58 was expressed in subplate neurons (arrows in Fig. 5F), but not in Cajal-Retzius cells (Fig. 5G; Supplementary Fig. 8). RP58 was not detected in Dlx2-positive cells (arrows in Fig. 5I), which correspond to GABAergic neurons. In the E16.5 hippocampus, RP58 was detected in most developing neurons and in some progenitor cells in the VZ (Fig. 5J). At E18.5, RP58 was detected in migrating neurons, pyramidal layer cells of the CA, and dentate granule cells (Fig. 5K), which were identified by immunoreactivity for NeuroD (Figs. 5L and L'). RP58 was not detected in reelin-positive Cajal-Retzius cells in the hippocampal fissure (asterisk in Fig. 5K). Therefore, RP58 is expressed in migrating and postmigratory glutamatergic neurons, which are impaired in the mutant, whereas RP58 is not expressed in the Cajal-Retzius cells and GABAergic neurons, which are not impaired in *RP58*-deficient animals, as shown in Fig. 2. Interestingly, RP58 is also expressed in the progenitor cells in the VZ. Interestingly, some cells in the VZ expressed the RP58 protein at a high level (arrows in Fig. 5H; Supplementary Figs. 7A–B'''), and other cells expressed this protein at a low level (arrowheads in Supplementary Figs. 7A–B'''). As all of these cells were positive for Ki67, a nuclear protein expressed only in cycling cells, this result suggests that RP58 is expressed by neural progenitors.

To examine whether the VZ cells that express RP58 are RGPs and/or IMPs, we performed double labeling of RP58 with Pax6 (which is an RGP marker) and Tbr2 (which is a pan-IMP marker). Most of the RP58-positive cells in the VZ were Tbr2-positive (arrows in Supplementary Figs. 9C–C'''), whereas some RP58-positive cells were Pax6-positive (arrows in Supplementary Figs. 9A–B''') and the others were Pax6-negative (arrowhead in Supplementary Figs. 9A–B'''). RP58 was expressed in P-H3-positive cells in the basal regions of the VZ, but not in the apical region of the VZ (Supplementary Fig. 10). RP58 was also detected in some of Ngn2-positive cells (Supplementary Fig. 11). These results suggest that the onset of RP58 expression happens during the transition from Pax6-positive cells to Tbr2-positive cells, or, in other words, at the initial stage of IMPs.

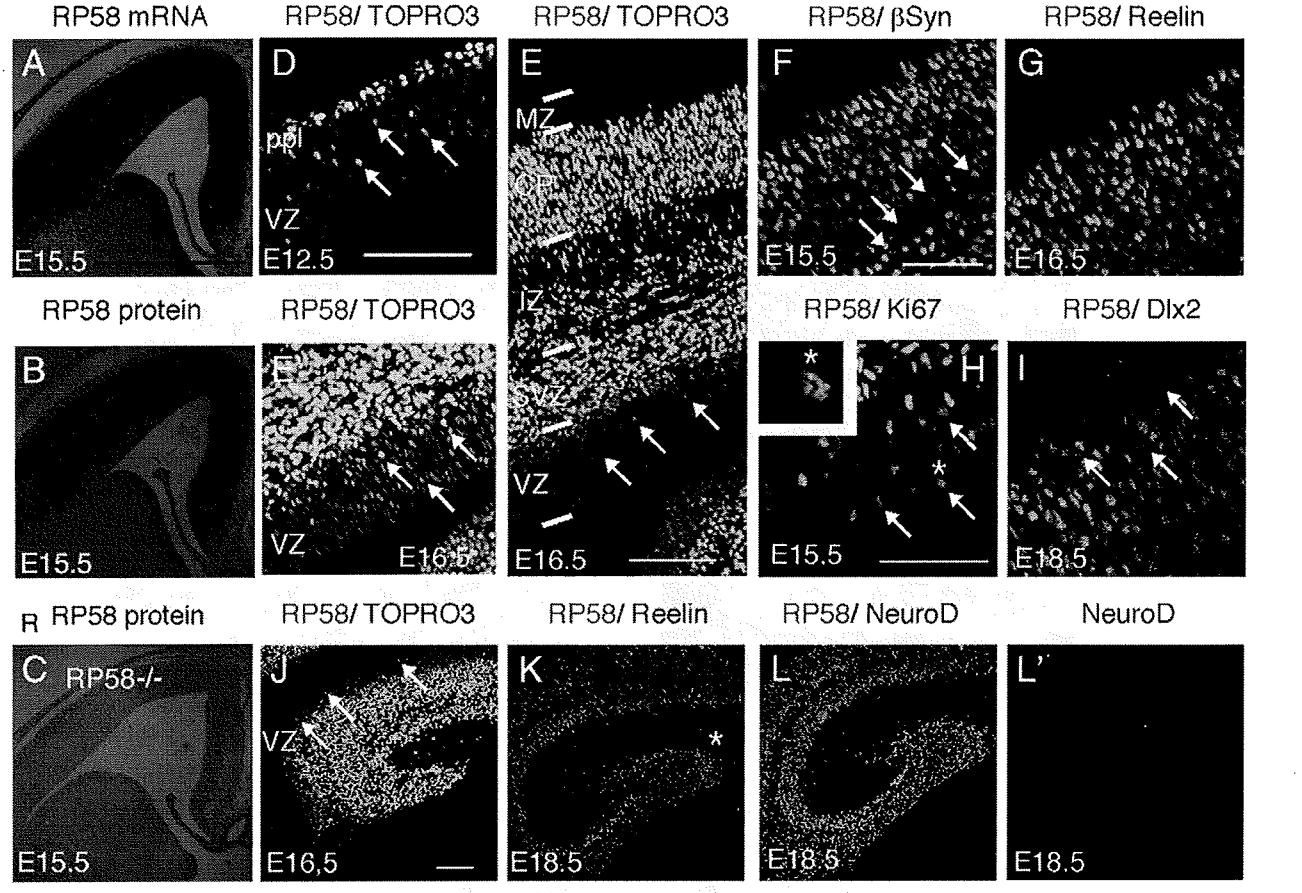

Fig. 5. RP58 expression patterns in the wild-type cerebral cortex. (A) RNA *in situ* hybridization analysis shows that RP58 transcripts were strongly expressed in cortical cells in the CP, IZ, SVZ, and weakly in the VZ of E15.5 wild-type mice. (B and C) RP58 protein was detected at high levels in the CP, IZ, and SVZ, and weakly in the VZ of E15.5 wild-type mice (B). No signal was detected in *RP58*$^{-/-}$ brain (C). (D, E, and E') RP58 protein was intensely expressed in developing neurons in the preplate (ppl) at E12.5 (D), in the CP, IZ, and SVZ at E16.5 (E), and in progenitor cells in the VZ at E12.5 (arrows in D) and E16.5 (arrows in E and E'). (F–I) RP58 was detected in β-synuclein-positive subplate neurons at E15.5 (F) and was not detected in the reelin-positive Cajal-Retzius cells at E16.5 (G). Ki67, which is a cell cycling marker, was detected in RP58-positive cells in the VZ at E15.5 (H). A higher magnification view of the region marked by an arrow with an asterisk (*) indicates that RP58 protein was expressed in Ki67-positive progenitor cells. RP58 was not detected in Dlx2-positive GABAergic neurons in the E18.5 neocortex (I). (J) RP58 was expressed in progenitors cells in the VZ (arrows in J) and in the developing neurons of the E16.5 hippocampus. (K–L') RP58 was not detected in reelin-positive Cajal-Retzius cells in the hippocampal fissure (asterisk, K) at E18.5. RP58 was detected in NeuroD-positive DG granule cells (L, L') at E18.5. Scale bars, 1 mm (A–C); 0.1 mm (D and E'), (E), and (J–L'); and 0.05 mm (F, G and I), (H).

Enhanced apoptosis in the RP58-deficient cortex

Next, we examined whether enhanced cell death or reduced production of cortical neurons in the mutant cortex were responsible for the fewer numbers of mature subplate and specified CP neurons observed in the mutant cortex. A larger number of TUNEL-positive cells were found in the postmitotic zone of the mutant neocortex at E15.5 and E18.5 when compared with the wild type, but no differences were observed in the proliferative zone (Figs. 6A, B, E, and F; Supplementary Fig. 12). The mutant hippocampus displayed a significant increase in the number of TUNEL-positive cells at E18.5 when compared with the wild type (Figs. 6M and N). Active-caspase3 immunoreactivity was also enhanced at E16.5 (Figs. 6C, D, I, and J) and E19 (Figs. 6G, H, O, and P) in both the neocortex and the hippocampus of the mutant mice, which suggests that caspase-dependent apoptosis is enhanced in the mutant. Apoptosis was detected in the anterior and posterior neocortex to the same degree (data not shown). Furthermore, single-strand DNA (ssDNA) staining using an anti-ssDNA antibody documented the presence of fragmented DNA (Figs. 6K and L), which confirmed the results of the TUNEL analysis. These results suggest that *RP58* deficiency enhances caspase-dependent apoptosis in the cerebral cortex, which may reduce the number of mature cortical neurons.

Expansion of the VZ/SVZ in the RP58-deficient cortex

In addition to enhanced apoptosis, we found that the VZ was likely to be expanded in the postnatal day (P) 0 mutant cortex (asterisk in Fig. 1B). We therefore examined the expression of several markers of the VZ, which included Pax6 (Englund et al., 2005). Pax6 expression expanded radially in the mutant cortex at E19 when compared with the distribution of this protein in the wild-type cortex at E19, as did PCNA immunoreactivity (Figs. 7A–B"). Furthermore, the expression of HES5, which is a basic helix–loop–helix transcription repressor expressed in the VZ (Ohtsuka et al., 2006), and of Tailless, which is an orphan nuclear receptor restricted to the VZ (Monaghan et al., 1995), was also enhanced in the mutant neocortex (Figs. 7C–F). The VZ was expanded in the hippocampus as well as in the neocortex, as determined by double staining of Pax6 with PCNA or Ki67 at E18.5 (Supplementary Fig. 13).

Next, we examined whether IMPs were increased in the mutant. Tbr2-positive cells, which are detected in IMPs and postmitotic immature neurons (Englund et al., 2005), were increased in the E18.5 mutant (Supplementary Figs. 14A and B). The phosphohistone H3 (P-H3)-positive mitotic cells in the SVZ, which correspond to mitotic cells of IMPs, were also increased, together with PCNA-positive cells (see Supplementary Figs. 14C–D'). These results suggest that IMPs were

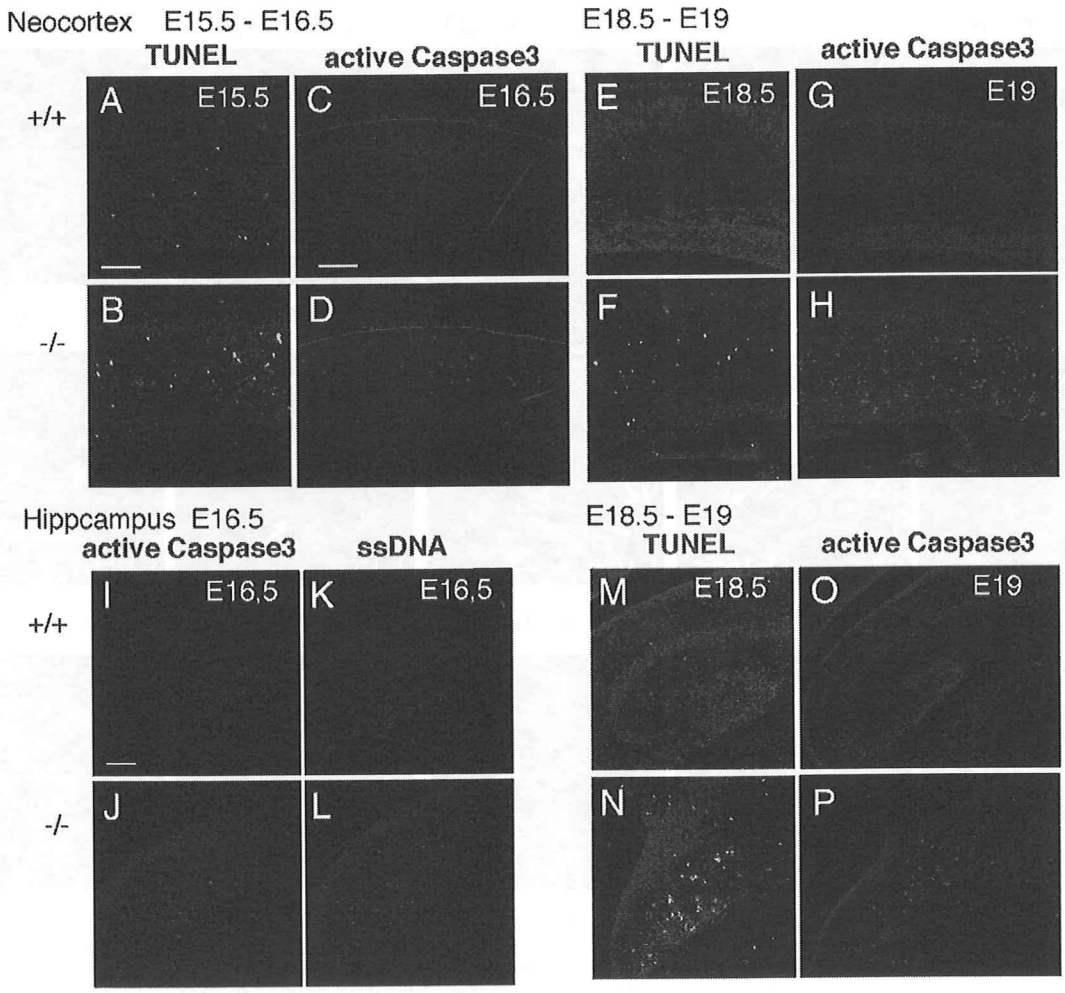

Fig. 6. Enhancement of apoptosis in the *RP58*-deficient cortex. (A–H) In the mutant neocortex, the number of TUNEL-positive cells was higher than in wild type at E15.5 (A and B) and E18.5 (E and F), and the number of active-caspase 3-positive cells was higher at E16.5 (C and D) and E19 (G and H). (I–P) In the mutant hippocampus, active-caspase 3-positive cells (I and J) and ssDNA-positive cells (K and L) were increased at E16.5 and TUNEL-positive cells and active-caspase 3-positive cells were also increased at E18.5 (M–P). Scale bars, 0.1 mm (A, B, E, F, M, and N), (C, D, G, H, O and P), and (I–L).

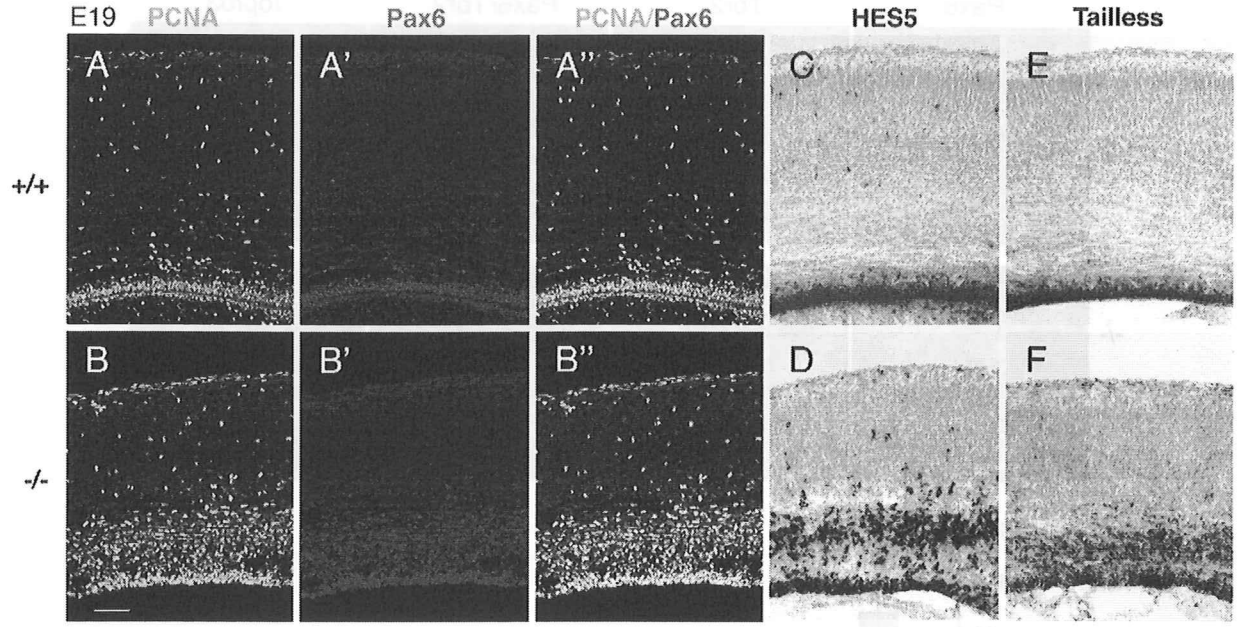

Fig. 7. Expansion of the ventricular zone in the *RP58*-deficient cortex. (A–B") PCNA-positive cells and Pax6-positive cells were increased in the $RP58^{-/-}$ cortex (A–B') and most Pax6-positive cells were immunoreactive for PCNA (A" and B"). (C–F) The $RP58^{-/-}$ cortex (D and F) exhibited more HES5-positive cells (C and D) and Tailless-positive cells (E and F) than the wild-type cortex (C and E). Scale bar, 0.1 mm (A–F).

increased in the mutant. To examine the developmental stage of IMPs, we performed double staining of Tbr2 and Pax6 (Fig. 8), as Pax6+/Tbr2+ cells and Pax6−/Tbr2+ cells are early-stage IMPs and late-stage IMPs, respectively (Sasaki et al., 2008). The double staining revealed that, in the E18.5 mutant, Tbr2-positive cells and Pax6-positive cells were increased in number, that both Pax6+/Tbr2− cells and Pax6+/Tbr2+ cells were also increased, whereas Pax6−/Tbr2+ cells were not (Fig. 8). This result suggests that RGPs and early-stage IMPs were increased in the mutant, whereas late-stage IMPs were not. To examine the identify of the SVZ, we preformed Svet1 *in situ* hybridization near the section of the Pax6/Tbr2 double staining from E15.5 to E18.5, which revealed that impairment of the mutant VZ/SVZ progressed from E15.5 to E18.5 (Supplementary Fig. 15). In particular, a tripartite appearance of inner Pax6-dominant/intermediate Tbr2-dominant/outer Pax6-dominant zones was observed in the mutant in later developmental stages (Supplementary Fig. 15). To directly associate these zones with Svet1 expression, we performed a triple staining of Pax6, Tbr2, and Unc5d that corresponds to Svet1 (Sasaki et al., 2008) (Supplementary Fig. 16). Unc5d/Svet1 staining was detected in the upper region of the Tbr2-positive zone in the wild type, while it was also detected, albeit weakly and diffusely, in the upper region of the intermediate Tbr2-positive zone and contained the outer Pax6-dominant zones in the E16.5 mutant mice (Supplementary Figs. 16 A–B'), which suggests that the outer Pax6-dominant zone was located in the SVZ. In the E18.5 mutant, the expression of Unc5d/Svet1 was more diffusely detected in the outer Pax6-dominant/intermediate Tbr2-dominant zone, which suggests that the mutant VZ/SVZ was severely impaired in the late development stages of the mutant (Supplementary Figs. 16 C–D').

The impairment of cell-cycle exit in the RP58-deficient VZ/SVZ during late development

We next examined whether the expansion of the VZ/SVZ of the mutant cortex was due to enhanced proliferation and/or impairment of cell-cycle exit. To examine cell proliferation, we counted the number of BrdU-labeled cells in a random selection of 50 Ki67 (which is a proliferating cell marker)-positive cells (which are considered to be progenitor cells) after a 30 min pulse of BrdU. The percentage of progenitor cells labeled with BrdU was not altered in the mutant cortex at E15.5, which suggests that proliferation was not altered in the mutant cortex (Figs. 9A–C). To examine the possibility that the division pattern of progenitor cells was impaired in the mutant cortex, we counted the number of PCNA-negative and Pax6-negative cells in a random selection of 50 BrdU-labeled cells, after a 24 h pulse of BrdU; this corresponds to the fraction of cells exiting the cell cycle. At E16.5, we found that the PCNA−/BrdU+ and Pax6−/BrdU+ ratios were about halved in *RP58* mutant progenitor cells when compared with their normal counterparts, which suggests that cell-cycle exit is inhibited in the mutant VZ progenitor cells in both the medial and lateral neocortices (Figs. 9D–I). This was confirmed by examining the total number of BrdU-positive cells in an area of 0.25 mm^2, which showed an increase in the number of PCNA− or Pax6+ cells; this suggests that reentry into the cell cycle is enhanced in the mutants (Supplementary Fig. 17). Furthermore, as the characteristic outer Pax6-dominant zone was observed in the mutant cortex (Supplementary Fig. 16B), we examined whether the outer Pax6-dominant zone was involved in the reduction of cell-cycle exit. The Pax6−/BrdU+ ratio was dominantly reduced in the upper region (IZ/SVZ), which contained the abnormal outer Pax6-dominant, when compared with the lower region (VZ) (Supplementary Fig. 18). Therefore, it is possible that the abnormal outer Pax6-dominant zone observed in the mutant reflects the reduction of cell-cycle exit. In contrast, neither proliferation at E12.5 (Supplementary Figs. 19A–C) nor cell-cycle exit at E13.5 (Supplementary Figs. 19D–I) was impaired. These results suggest that cell-cycle exit is reduced in the mutant cortex at late neocorticogenesis. The reduction of the cell-cycle exit causes an increase in VZ progenitor cells and thereby leads to the expansion of the VZ. Therefore, it is likely that the reduction of cell-cycle exit, in addition to the enhanced apoptosis, decreases the number of differentiated late-born neurons in the mutant CP.

As cell-cycle kinetics may affect cell-cycle exit, we estimated the duration of the S-phase (Ts) and of the total cell-cycle time (Tc) using a BrdU/IdU double labeling paradigm (Martynoga et al., 2005), which revealed no obvious differences in Ts, Tc, and Ts/Tc between wild-type and mutant cortices (Supplementary Fig. 20); however, because this

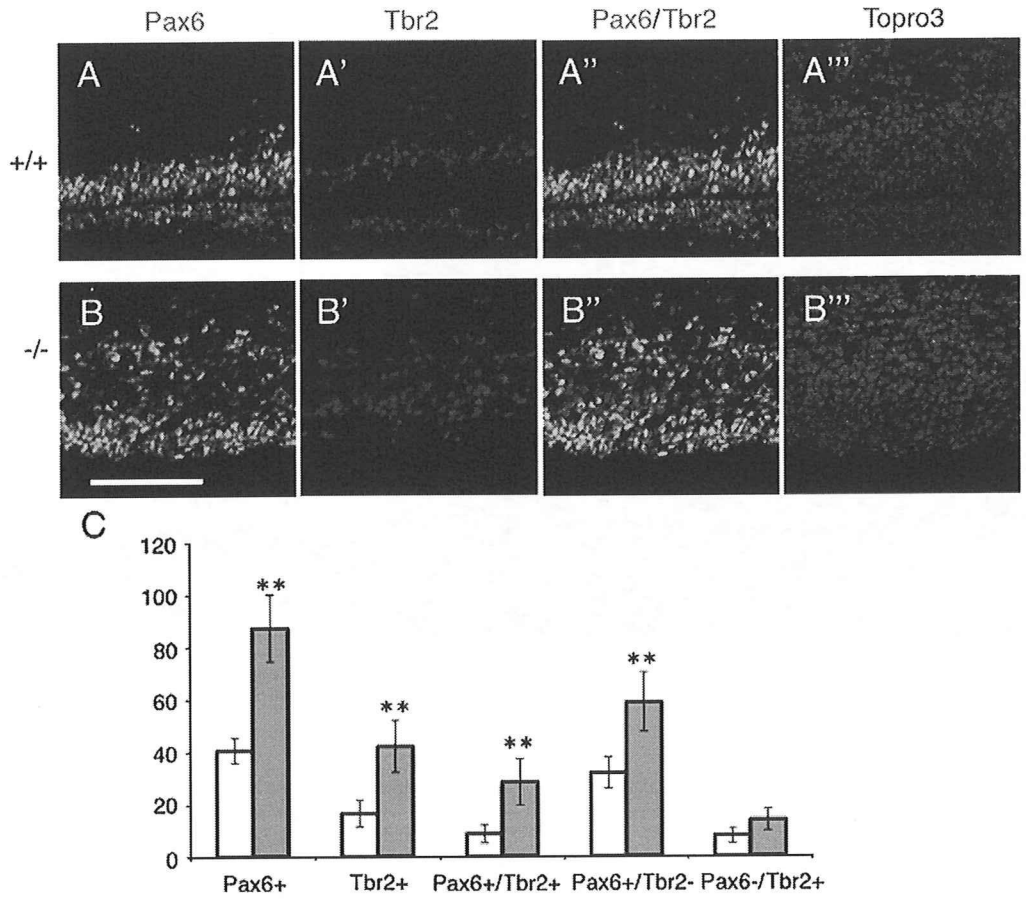

Fig. 8. Both Pax6-positive and Tbr2-positive cells were increased in the *RP58*-deficient cortex. Double staining (A'', B'') of Pax6 (A, B) and Tbr2 (A', B') with the TOPRO3 nuclear stain (A''', B''') showed that both Pax6-positive and Tbr2-positive cells were increased in the *RP58*-deficient cortex. Scale bars, 0.1 mm (A–B'''). (C) The number of Pax6+, Tbr2+, Pax6+/Tbr2+, Pax6+/Tbr2−, and Pax6−/Tbr2+ cells was counted in a 0.0083 mm^2 area of the wild-type (open column) and of the mutant neocortex (gray column). Faint staining of Pax6 was regarded as negative. Six regions of three mutant brains were compared with six regions of three wild-type brains. The data are presented as means ± SD. $^{**}P<0.01$ (Student's *t* test).

estimation rested on the assumption that all cells in the VZ are proliferating and that the precursor cells consist of a single proliferating population with the same cycling kinetics (Martynoga et al., 2005), further analyses may be necessary to assess the possibility that RP58 is involved in cell-cycle kinetics.

Discussion

In the present study, we characterized mice carrying disrupted alleles for the POZ/zinc finger transcriptional repressor gene, *RP58*. We found that homozygous mutants display severe hypoplasia of the cerebral cortex and of the hippocampus, in association with enhanced apoptosis and expansion of the VZ/SVZ. We showed that RP58 is specifically required for the maturation and survival of the excitatory neurons of the cerebral cortex. Furthermore, the present study demonstrated that RP58 is a novel factor that controls the balance of cell division of neuronal progenitors, which remains poorly understood to date.

In the *RP58* null mutant, the VZ was expanded and the dorsal cortex appeared like a wild-type younger brain. Therefore, the possibility of developmental delay cannot be excluded. We examined the expression of Tbr1 in the mutant cortex at E13.5, E15.5, and E18.5, which suggested that there is no clear time lag in the Tbr1 expression pattern (Supplementary Fig. 3). In addition, the Tc may cause a developmental delay. The Tc was not altered in the *RP58*-deficient mice (Supplementary Fig. 20). These results do not support the contention that developmental delay mainly occurs in *RP58* null mice. It seems more likely that reduction of produced matured neurons and enhancement of apoptosis causes the impairment in cortical development observed in these animals.

One of the main phenotypes in the *RP58*-deficient cortex was a reduction in the number of mature cortical neurons. In addition to a substantial reduction in the number of neurons in the subplate and layers 2–5 of the CP in the neocortex, Tbr1 expression was strongly suppressed throughout the cortical anlage, with the exception of the Cajal-Retzius cells in the hippocampus. The pyramidal layer of the CA was absent and Tbr1 expression was severely reduced in NeuroD-positive granule cells of the DG. NeuroD is expressed after Pax6, but before Tbr1 (Hevner et al., 2006), which suggests that *RP58* deficiency suppresses the production of mature dentate granule neurons.

In the early embryonic stage, *RP58* deficiency did not impair cell-cycle exit, although apoptosis was enhanced in the mutant neocortex at E15. Therefore, the decreased number of mature subplate neurons produced at early embryonic stages could be caused by enhanced apoptosis. On the other hand, the VZ was expanded at later embryonic stages in the mutant, the cell-cycle exit was inhibited in RGPs, and the level of apoptosis remained high, which suggest that enhanced apoptosis and/or defective cell-cycle control reduce the production of mature cortical neurons at later development stages.

Transgenic mice expressing β-catenin precursors also show reduced cell-cycle exit and develop enlarged brains with reduced cortical thickness (Chenn and Walsh, 2002). In contrast, $RP58^{-/-}$ mice showed no enlargement of the brain, although the thickness of the neocortex was reduced. This discrepancy may be due to the reduction

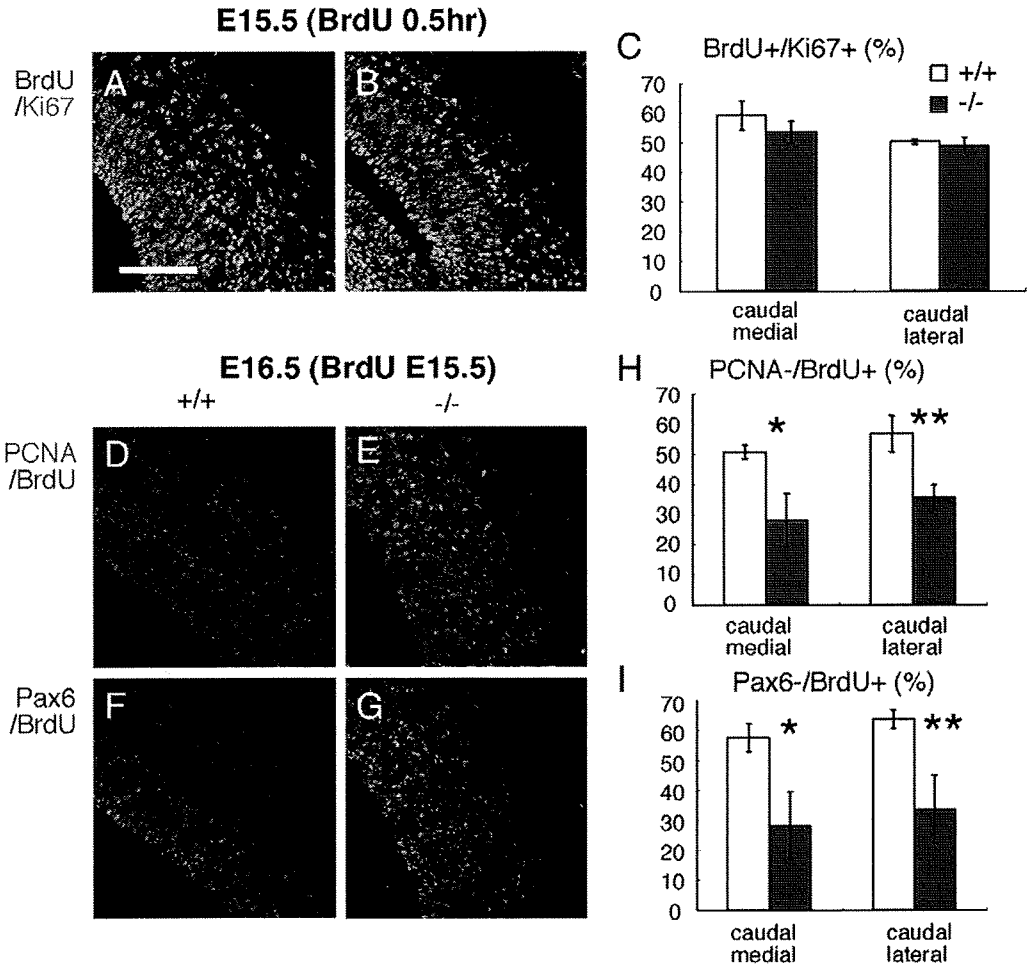

Fig. 9. Impairment of cell-cycle exit in the *RP58*-deficient cortex in late neocortical development. (A–C) Double labeling with BrdU and Ki67 in the lateral region of the wild-type (A) and mutant (B) caudal neocortex at E15.5, 0.5 h after BrdU incorporation. The fraction of BrdU-positive cells among the Ki67-positive cells was not altered in the medial and lateral regions of the mutant cortex (C), which suggests that proliferation is not affected in the mutant cortex. Fifty Ki67-positive cells were randomly examined. Four regions of two mutant brains were compared with six regions of three wild-type brains. (D–I) BrdU was incorporated at E15.5 and the lateral region of the caudal neocortex was double stained for BrdU and PCNA (D and E) or Pax6 (F and G) in the lateral region of the wild-type (D and F) and the mutant (E and G) at E16.5. The fraction of PCNA-negative cells and Pax6-negative cells among the BrdU-positive cells was reduced in the caudal *RP58*-deficient cortex in both the medial and lateral regions of the mutant caudal neocortex (H and I), which suggests that cell-cycle exit was reduced. Fifty BrdU-positive cells were randomly examined. Three regions of three mutant brains were compared with three regions of three wild-type brains. Scale bar, 0.1 mm (A–D, G, and H). The data are presented as means ± SD. $*P<0.02$, $**P<0.01$ (Student's *t* test).

of cell-cycle exit only at late embryonic stages and/or the presence of high levels of apoptosis in the $RP58^{-/-}$ cortex. We consider RP58 a candidate molecule for the control of the number of mature cortical neurons, as *RP58* deficiency decreased the number of mature neurons because of enhanced apoptosis and of defects in cell-cycle exit.

A delicate balance in cell proliferation and subsequent cell-cycle withdrawal and differentiation into specific neurons is essential for corticogenesis. The present study indicates the possibility that RP58 regulates this balance, at least at the late embryonic stage. In the wild-type E15.5 VZ, some RP58-positive cells showed weak Pax6 immunoreactivity, and almost all RP58-positive cells exhibited Tbr2 immunoreactivity (Supplementary Fig. 9), which suggests that the onset of RP58 expression happens in IMPs, at the initial stage, when Pax6 and Tbr2 may be coexpressed (Englund et al., 2005).

Pax6+ cells were increased in the *RP58* null mutant, as were both Pax6+/Tbr2− and Pax6+/Tbr2+ cells. The increase in the number of Pax6+/Tbr2− cells in the mutant is explained by the reduction of cell-cycle exit of VZ progenitors. It is likely that there are extrinsic actions that allow RP58 to activate the expression of extrinsic factors that control cell-cycle exit, because RP58 is not detected in most Pax6+ cells. In fact, it is reported that the generation of projection neurons from cortical progenitors appears to be governed by both cell-intrinsic and environmental cues (Mizutani and Gaiano, 2006); however, we cannot exclude the possibility that a few Pax6+ cells abnormally proliferated in the mutant, as RP58 was detected in some Pax6+ cells in the wild type.

Pax6+/Tbr2− and Pax6+/Tbr2+ cells were increased in the mutant VZ/SVZ, whereas Pax6−/Tbr2+ cells were not increased. Therefore, it is possible that Pax6 is ectopically expressed in Tbr2+ IMPs in the mutant, and that the transition from Pax6+/Tbr2+ cells to Pax6−/Tbr2+ cells was inhibited in the mutant, which raises the possibility that RP58 may be an important molecule for the maturation of IMPs. It was reported that (1) Svet1 is a spliced intronic sequence from Unc5d (Sasaki et al., 2008) and (2) Svet1/Unc5d staining is a specific marker of late-stage IMPs. It is likely that Svet1/Unc5d expression was reduced in the mutant, which supports the possibility that RP58 is most important for maturation process from early-stage IMPs to late-stage IMPs; however, as the expression of Svet1/Unc5d is also observed in young neurons (Kawaguchi et al., 2008), the possibility that the reduction of Svet1/Unc5d signal in the mutant reflects the reduction of the number of generated neurons cannot be excluded.

The expression of Pax6, Tbr2, and Svet1/Unc5d reveals that the formation of VZ/SVZ was impaired in the mutant (Supplementary Figs. 15 and 16). The outer Pax6-dominant zone in the E16.5 mutant may be caused by the reduced cell-cycle exit (Supplementary Fig. 18). The outer Pax6-dominant zone in E16.5 was not distinct when compared with that of the E18.5 animals. Therefore, the outer Pax6-dominant zone observed in the E18.5 mutant may partially explain the reduced cell-cycle exit.

Tbr2-positive cells were increased in the mutant VZ/SVZ, as were Pax6+/Tbr2+ cells, but not Pax6−/Tbr2+ cells. Tbr2+ IMPs are originated from Pax6+ RGPs. Therefore, the increase in Pax6+/Tbr2+ cells in the mutant may be explained by the increase in Pax6+/Tbr2− cells.

We showed that RP58 was expressed in some Ngn2-positive cells (Supplementary Fig. 11). RP58 acts downstream of Ngn2 (Seo et al., 2007), which is involved in the initial commitment to a neuronal fate. Therefore, RGPs neuronally committed by Ngn2 probably express RP58 in the VZ in a sustained manner. As RP58 functions as a transcriptional repressor, it is possible that RP58 suppresses the expression of a few genes, which may include *Pax6*, *Tbr2*, and *Ngn2*. *In vitro* analysis indicated that the transcription of Ngn2 was suppressed by RP58 and that Ngn2-positive cells were increased in the *RP58*-null mutant cortex (data not shown; Ohtaka-Maruyama et al., in preparation). It was reported that Tbr2 is a target of Ngn2 (Ochiai et al., 2009). Therefore, the increase in Tbr2-positive cells in the *RP58* mutant can be explained by the enhancement of Ngn2 expression, probably because of a lack of transcriptional suppression by RP58.

On the other hand, the overexpression of some genes, which include *Pax6*, *Tbr2*, and *Ngn2*, may explain the abnormalities observed in the *RP58*-deficient brain. The overexpression of *Pax6* affects the proliferation of neuronal progenitors and causes failure of neuronal differentiation (Bel-Vialar et al., 2007) and Tbr2 misexpression inhibits cell-cycle exit (Sessa et al., 2008). We are now analyzing whether the phenotype of the *RP58* mutant brain can be explained by the enhanced expression of those genes.

In conclusion, we found that RP58 deficiency reduces the number of mature cortical neurons via strongly enhanced apoptosis and impaired cell-cycle exit, which suggests that RP58 plays a key role in the survival of cortical neurons and in the development of neuronal progenitors.

Acknowledgments

We thank Drs. Koki Kawamura, Makoto Hashimoto, Minoru Saitoe, Junjiro Horiuchi (Tokyo Metropolitan Institute for Neuroscience (TMIN)), Douglas E. Vetter (Tufts University School of Medicine), and Mitsuharu Hattori (Nagoya City University) for critical suggestions. We also thank Dr. Kazuaki Yoshikawa (Osaka University) for the guinea pig anti-Dlx2 antibody and Dr. David Anderson (California Institute of Technology) for the mouse anti-Neurogenin2 antibody. We thank Drs. Yoshinobu Sugitani and Tetsuo Noda (JFCR-Cancer Institute) for providing the mouse *CTGF*, mouse *Tailless*, mouse *Tbr1*, and mouse *SorLA* cDNAs used to prepare the probes for RNA *in situ* hybridization, as well as Dr. Thomas M. Jessell (Columbia University Medical Center) for mouse *ER81*, Dr. Susan K. McConnell (Stanford University) for mouse *RORβ*, Dr. Victor Tarabykin (Max Planck Institute of Biophysical Chemistry) for *Svet1*, Dr. Shinichi Aizawa (RIKEN Kobe) for *NT3*, Dr. Greg E. Lemke (Salk Institute) for *SCIP*, Dr. Jim Boulter (UCLA Brain Research and Molecular Biology Institutes) for *KA1*, and Dr. Francois Guillemot (NIMR) for *HES5* cDNAs. We also thank Ms. Yasuko Kishimoto (Histology Center, TMIN) for her technical assistance. These studies were supported by a grant-in-aid from the Ministry of Science, Education and Culture to H. O. and by Human Science Research Funds and the Budget for Nuclear Research of the MEXT, awarded to M. K.

Appendix A. Supplementary data

Supplementary data associated with this article can be found, in the online version, at doi:10.1016/j.ydbio.2009.04.030.

References

Allendoerfer, K.L., Shatz, C.J., 1994. The subplate, a transient neocortical structure: its role in the development of connections between thalamus and cortex. Annu. Rev. Neurosci. 17, 185–218.
Aoki, K., Meng, G., Suzuki, K., Takashi, T., Kameoka, Y., Nakahara, K., Ishida, R., Kasai, M., 1998. RP58 associates with condensed chromatin and mediates a sequence-specific transcriptional repression. J. Biol. Chem. 273, 26698–26704.
Arber, S., Ladle, D.R., Lin, J.H., Frank, E., Jessell, T.M., 2003. EST gene Er81 controls of formation of functional connection between group Ia sensory afferents and motor neurons. Cell 101, 485–498.
Bayer, S.A., Altman, J., 1991. Neocortical Development. Raven Press.
Buaas, F.W., Kirsh, A.L., Sharma, M., McLean, D.J., Morris, J.L., Griswold, M.D., de Rooji, D. G., Braun, R.E., 2004. Plzf is required in adult male germ cells for stem cell self-renewal. Nat. Genet. 36, 647–652.
Bel-Vialar, S., Medevielle, F., Pituello, F., 2007. The on/off of Pax6 controls the tempo of neuronal differentiation in the developing spinal cord. Dev. Biol. 305, 659–673.
Bettler, B., Boulter, J., Hermanss-Borgmeyer, U., Hollmann, M., Heinemann, S., 1990. Cloning of a novel glutamate receptor subunit, GluR5: expression in the nervous system during development. Neuron 5, 583–595.
Cau, E., Gradwohl, G., Casarosa, S., Kageyama, R., Guillemot, F., 2000. Hes genes regulate sequential stages of neurogenesis in the olfactory epithelium. Development 127, 2323–2332.
Chenn, A., Walsh, C.A., 2002. Regulation of cerebral cortical size by control of cell cycle exit in neural precursors. Science 297, 365–369.
Costoya, J.A., Hobbs, R.M., Barna, M., Cattoretti, G., Monava, K., Sukhwani, M., Orwig, K.E., Wolgemuth, D.J., Pandolfi, P.P., 2004. Essential role Plzf in maintenance of spermatogonial stem cells. Nat. Genet. 36, 653–659.
Dehay, C., Kennedy, H., 2007. Cell-cycle control and cortical development. Nat. Rev. Neurosci. 8, 438–450.
Englund, C., Fink, A., Lau, C., Pham, D., Daza, R.A.M., Bulfone, A., Kowalczyk, T., Hevner, R. F., 2005. Pax6, Tbr2, and Tbr1 are expressed sequentially by radial glia, intermediate progenitor cells, and postmitotic neurons in developing neocortex. J. Neurosci. 25, 247–251.
Forster, E., Zhao, S., Frotscher, M., 2006. Laminating the hippocampus. Nat. Rev. Neurosci. 7, 259–267.
Frantz, G.D., Bohner, A.P., Akers, R.M., McConnell, S.K., 1994. Regulation of the POU domain gene SCIP during cerebral cortical development. J. Neurosci. 14, 472–485.
Friedman, W.J., Ernfors, P., Persson, H., 1991. Transient and persistent expression of NT-3/HDNF mRNA in the rat brain during postnatal development. J. Neurosci. 11, 1577–1584.
Friedrichsen, S., Heuer, H., Christ, S., Winckler, M., Brauer, D., Bauer, K., Raivich, G., 2003. CTGF expression during mouse embryonic development. Cell Tissue Res. 312, 175–188.
Friocourt, G., Kanatani, S., Tabata, H., Yozu, M., Takahashi, T., Antypa, M., Raguénès, O., Chelly, J., Férec, C., Nakajima, K., Parnavelas, J.G., 2008. Cell-autonomous roles of ARX in cell proliferation and neuronal migration during corticogenesis. J. Neurosci. 28, 5794–5805.
Fuks, F., Burgers, W.A., Godin, N., Kasai, M., Kouzarides, T., 2001. Dnmt3a binds deacetylases and is recruited by a sequence-specific repressor to silence transcription. EMBO J. 10, 2536–2544.
Fukuda, T., Kawano, H., Ohyama, K., Li, H.P., Takeda, Y., Oohira, A., Kawamura, Y., 1997. Immunohistochemical localization of neurocan and L1 in the formation of thalamocortical pathway of developing rat. J. Comp. Neurol. 382, 141–152.
Funatsu, N., Inoue, T., Nakamura, S., 2004. Gene expression analysis of the late embryonic mouse cerebral cortex using DNA microarray: identification of several region- and layer-specific genes. Cereb. Cortex 14, 1031–1044.
Galichet, C., Guillemot, F., Parras, C.M., 2008. Neurogenin 2 has an essential role in development of the dentate gyrus. Development 135, 2031–2041.
Gebhardt, A., Kosan, C., Herkert, B., Möröy, T., Lutz, W., Eilers, M., Elsässer, H.P., 2007. Miz1 is required for hair follicle structure and hair morphogenesis. J. Cell. Sci. 120, 2586–2593.
Hashimoto, M., Rockenstein, E., Mante, M., Mallory, M., Masliah, E., 2001. β-synuclein inhibits α-synuclein aggregation: a possible role as an anti-parkinsonian factor. Neuron 32, 213–223.
Haubensak, W., Attardo, A., Denk, W., Huttner, W.B., 2004. Neurons arise in the basal neuroepithelium of the early mammalian telencephalon: a major site of neurogenesis. Proc. Natl. Acad. Sci. U. S. A. 101, 3196–3201.
Hermans-Borgmeyer, I., Hampe, W., Schinke, B., Methner, A., Nykjaer, A., Süsens, U., Fenger, U., Herbarth, B., Schaller, H.C., 1998. Unique expression pattern of a novel mosaic receptor in the developing cerebral cortex. Mech. Dev. 70, 65–76.
Heuer, H., Christ, S., Friedrichsen, S., Brauer, D., Winckler, M., Bauer, K., Raivich, G., 2003. Connective tissue growth factor: a novel marker of layer VII neurons in the rat cerebral cortex. Neuroscience 119, 43–52.
Hevner, R.F., Hodge, R.D., Daza, R.A.M., Englund, C., 2006. Transcription factor in glutamatergic neurogenesis: conserved program in neocortex, cerebellum, and adult hippocampus. Neurosci. Res. 55, 223–233.
Ishida, R., Okado, H., Sato, H., Shionoiri, C., Aoki, K., Kasai, M., 2002. A role for the octameric ring protein, Translin, in mitotic cell division. FEBS Lett. 525, 105–110.

Kawaguchi, A., Ikawa, T., Kasukawa, T., Ueda, H.R., Kurimoto, K., Saitou, M., Matsuzaki, F., 2008. Single-cell gene profiling defines differential progenitor subclasses in mammalian neurogenesis. Development 135, 3113–3124.
Kawano, H., Fukuda, T., Kubo, K., Horie, M., Uyemura, K., Takeuchi, K., Osumi, N., Eto, K., Mawamura, K., 1999. Pax-6 is required for thalamocortical pathway formation in fetal rats. J. Com. Neurol. 408, 147–160.
Kelly, K.F., Daniel, J.M., 2006. POZ for effect-POZ-ZF transcription factors in cancer and development. Trends Cell Biol. 16, 578–587.
Kiefer, H., Chatail-Hermitte, F., Ravassard, P., Bayard, E., Brunet, I., Mallet, J., 2005. ZENON, a novel POZ Kruppel-like DNA binding protein associated with differentiation and/or survival of late postmitotic neurons. Mol. Cell. Biol. 25, 1713–1729.
Kuwajima, T., Nishimura, I., Yoshikawa, K., 2006. Necdin promotes GABAergic neuron differentiation in cooperation with Dlx homeodomain proteins. J. Neurosci. 26, 5383–5392.
Lee, S.M.K., Tole, S., Grove, E., McMahon, A.P., 2000. A local Wnt-3asignal is required for development of the mammalian hippocampus. Development 127, 457–467.
Li, G., Pleasure, S.J., 2007. Genetic regulation of dentate gyrus morphogenesis. Prog. Brain Res. 163, 143–152.
Martynoga, B., Morrison, H., David, J., Price, D.J., Mason, J.O., 2005. Foxg1 is required for specification of ventral telencephalon and region-specific regulation of dorsal telencephalic precursor proliferation and apoptosis. Dev. Biol. 283, 113–127.
Meng, G., Inazawa, J., Ishida, R., Tokura, K., Nakahara, K., Aoki, K., Kasai, M., 2000. Structural analysis of the gene encoding RP58, a sequence-specific transrepressor associated with heterochromatin. Gene 242, 59–64.
Meyer, G., Socorro, A.C., Garcia, C.G.P., Millan, L.M., Walker, N., Caput, D., 2004. Developmental roles of p73 in Cajal-Retzius cells and cortical patterning. J. Neurosci. 24, 9878–9887.
Miyata, T., Kawaguch, A., Saito, K., Kawano, M., Muto, T., Ogawa, M., 2004. Asymmetric production of surface-division and non-surface division cortical progenitor cells. Development 131, 3133–3145.
Mizutani, K., Gaiano, N., 2006. Chalk one up for 'nature' during neocortical neurogenesis. Nat. Neurosci. 9, 717–718.
Molyneaux, B.J., Arlotta, P., Menezes, J.R., Macklis, J.D., 2007. Neuronal subtype specification in the cerebral cortex. Nat. Rev. Neurosci. 8, 427–437.
Monaghan, A.P., Grau, E., Bock, D., Schutz, G., 1995. The mouse homolog of the orphan nuclear receptor tailless is expressed in the developing forebrain. Development 121, 839–853.
Nakajima, K., Mikoshiba, K., Miyata, T., Kudo, C., Ogawa, M., 1997. Disruption of hippocampal development in vivo by CR-50 mAb against Reelin. Proc. Natl. Acad. Sci. U. S. A. 94, 8196–8201.
Noctor, S.C., Martinez-Cerdeno, V., Ivic, L., Kringstein, A.R., 2004. Cortical neurons arise in symmetric and asymmetric division zones and migrate through specific phases. Nat. Neurosci. 7, 136–144.
Ochiai, W., Nakatani, S., Takahara, T., Kainuma, M., Masaoka, M., Minobe, S., Namihira, M., Nakashima, K., Sakakibara, A., Ogawa, M., Miyata, T., 2009. Periventricular notch activation and asymmetric Ngn2 and Tbr2 expression in pair-generated neocortical daughter cells. Mol. Cell Neurosci. 40, 225–233.
Ogawa, M., Miyata, T., Nakajimat, K., Yagyu, K., Seike, M., Ikenaka, K., Yamamoto, H., Mikoshiba, K., 1995. The *reeler* gene-associated antigen on Cajal-Retzius neurons is a crucial molecule for laminar organization of cortical neurons. Neuron 14, 899–912.
Ohtaka-Maruyama, C., Miwa, A., Kawano, H., Kasai, M., Okado, H., 2007. Spatial and temporal expression of RP58, a novel zinc finger transcriptional repressor, in mouse brain. J. Comp. Neurol. 502, 1098–1108.
Ohtsuka, T., Imayoshi, I., Shimojo, H., Nishi, E., Kageyama, R., McConnell, S., 2006. Visualization of embryonic neural stem cells using Hes promoters in transgenic mice. Mol. Cell. Neurosci. 31, 109–122.
Pleasure, S.J., Collins, A.E., Lowenstein, D.H., 2000. Unique expression pattern of cell fate molecule delinate sequential stages of dentate gyrus development. J. Neurosci. 20, 6095–6105.
Sasaki, S., Tabata, H., Tachikawa, K., Nakajima, K., 2008. The cortical subventricular zone-specific molecule Svet1 is part of the nuclear RNA coded by the putative Netrin receptor gene Unc5d and is expressed in multipolar migrating cells. Mol. Cell. Neurosci. 38, 474–483.
Seo, S., Lim, J.W., Yallajoshyula, D., Chang, L.W., Kroll, K.L., 2007. Neurogenin and NeuroD direct transcriptional targets and their regulatory enhancers. EMBO J. 26, 5093–5108.
Sessa, A., Mao, C.a., Hadjantonakis, A.K., Klein, W.H., Broccoli, V., 2008. Tbr2 directs conversion of radial glia into basal precursors and guides neuronal amplification by indirect neurogenesis in the developing neocortex. Neuron 60, 56–69.
Shinozaki, K., Yoshida, M., Nakamura, M., Aizawa, S., Suda, Y., 2004. Emx1 and Emx2 cooperate in initial phase of archipallium development. Mech. Dev. 121, 475–489.
Smart, I.H., McSherry, G.M., 1982. Growth patterns in the lateral wall of the mouse telencephalon. II. Histological changes during and subsequent to the period of isocortical neuron production. J. Anat. 34, 415–442.
Sugitani, Y., Nakai, S., Minowa, O., Nishi, M., Jishage, K., Kawano, H., Mori, K., Ogawa, M., Noda, T., 2002. Brn-1 and Brn-2 share crucial roles in the production and positioning of mouse neocortical neurons. Genes Dev. 16, 1760–1765.
Takahashi, A., Hirai, S., Ohtaka-Maruyama, C., Miwa, A., Hata, Y., Okabe, S., Okado, H., 2008. Co-localization of a novel transcriptional repressor simiRP58 with RP58. Biochem. Biophys. Res. Commun. 368, 637–642.
Tarabykin, V., Stoykova, A., Usman, N., Gruss, P., 2001. Cortical upper layer neurons derive from the subventricular zone as indicated by *Svet1* gene expression. Development 128, 1983–1993.
Weimann, J.M., Zhang, Y.A., Levin, M.E., Devin, W.P., Brulet, P., McConnell, S.K., 1999. Cortical neurons require Otx1 for the refinement of exuberant axonal projections to subcortical targets. Neuron 24, 819–831.

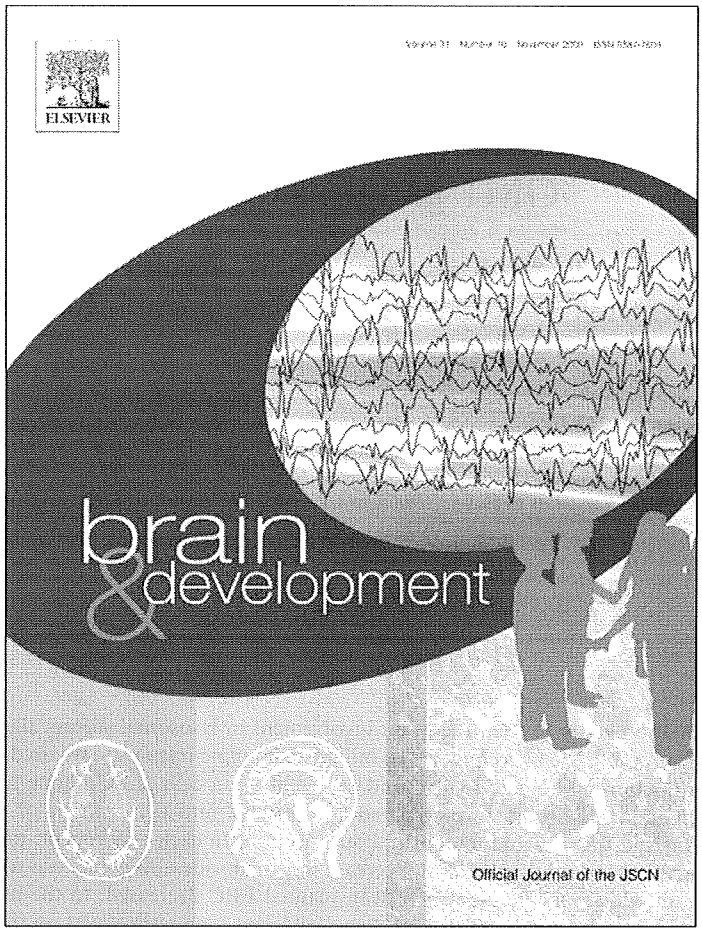

ELSEVIER

Brain & Development 31 (2009) 717–724

BRAIN & DEVELOPMENT
Official Journal of the Japanese Society of Child Neurology

www.elsevier.com/locate/braindev

Original article

Intracerebral cell transplantation therapy for murine GM1 gangliosidosis

Tomo Sawada [a], Akemi Tanaka [a,*], Katsumi Higaki [c], Ayumi Takamura [c], Eiji Nanba [c], Toshiyuki Seto [a,e], Mitsuyo Maeda [b], Etsuko Yamaguchi [a], Junichiro Matsuda [d], Tunekazu Yamano [a]

[a] *Department of Pediatrics, Osaka City University Graduate School of Medicine, 1-4-3 Asahi-machi, Abeno-ku, Osaka 545-8585, Japan*
[b] *Department of Neurobiology and Anatomy, Osaka City University Graduate School of Medicine, Osaka, Japan*
[c] *Division of Functional Genomics, Research Center for Bioscience and Technology, Tottori University, Yonago, Japan*
[d] *Laboratory of Experimental Animal Models, Division of Bioresources, National Institute of Biomedical Innovation, Osaka, Japan*
[e] *Department of Pediatrics, Fujiidera City Hospital, Fujiidera, Japan*

Received 25 August 2008; received in revised form 15 October 2008; accepted 1 November 2008

Abstract

We performed a cell transplantation study to treat the brain involvement in lysosomal storage diseases. We used acid β-galactosidase knock-out mice (BKO) from C57BL/6 as recipients. To minimize immune responses, we used cells derived from transgenic mice of C57BL/6 overexpressing the normal human β-galactosidase. Fetal brain cells (FBC), bone marrow-derived mesenchymal stem cells (MSC), and mixed FBC and MSC cells were prepared and injected into the ventricle of newborn BKO mouse brain. The mice were examined at 1, 2, 4, and 8 weeks and 6 months after injection. In each experiment, the injected cells migrated into the whole brain effectively and survived for at least 8 weeks. Decrease in ganglioside GM1 level was also observed. FBC could survive for 6 months in recipient brain. However, the number of transplanted FBC decreased. In the brains of MSC- or mixed cell-treated mice, no grafted cells could be found at 6 months. To achieve sufficient long-term effects on the brain, a method of steering the immune response away from cytotoxic responses or of inducing tolerance to the products of therapeutic genes must be developed.

Keywords: GM1-gangliosidosis; Cell transplantation; Fetal brain cell; Mesenchymal stem cell

1. Introduction

Enzyme replacement therapy (ERT), hematopoeitic stem cell transplantation (HSCT), and gene transfer have been studied in animals and in humans with lysosomal storage disease (LSD). ERT is now available clinically for Gaucher disease, Fabry disease, Pompe disease, and MPS I, II, and VI in many countries, and has been successful in visceral organs. HSCT is also effective against the somatic involvements in Gaucher disease and MPS I, II, and VI. However, HSCT exhibits little efficacy in conditions such as Fabry disease and Pompe disease, when enzyme secretion from donor cells is poor or the uptake of enzyme proteins by the affected host cells is inadequate. In addition, efficacy in individual organs differs markedly, in both ERT and HSCT, depending on accessibility of blood flow and the density of mannose-6-phosphate receptors. Neither HSCT nor ERT exhibits efficacy against the brain involvement in Gaucher or MPSs because of the poor access due to the blood–brain barrier.

Many experimental studies have been carried out, involving methods such as gene therapy [1–5], cell

* Corresponding author. Tel.: +81 6 6645 3816; fax: +81 6 6636 8737.
E-mail address: akemi-chan@med.osaka-cu.ac.jp (A. Tanaka).

0387-7604/$ - see front matter © 2008 Elsevier B.V. All rights reserved.
doi:10.1016/j.braindev.2008.11.004